INTERIM REPORT

Impact of Climate Change on Meteorology and Regional Air Quality in California

Contract # 04-349

Reporting Period: August – November 2005

Principal Investigators:
Michael Kleeman, UC Davis
Dan Cayan, Scripps Institution of Oceanography, UC San Diego

Prepared for:

State of California Air Resources Board
Research Division
PO Box 2815
Sacramento CA 95812

Contact Information:

Michael Kleeman
Department of Civil and Environmental Engineering
University of California
Davis, CA, 95616
(530) 752-8386

November, 2005

Disclaimer

The statements and conclusions of this Report are those of the contractor and not necessarily those of the California Air Resources Board. The mention of commercial products, their source, or their use in connection with material reported herein is not to be construed as actual or implied endorsement of such products.

Acknowledgment

This research was funded by the California Air Resources Board under Contract # 04-349. The authors gratefully acknowledge the assistance of Nehzat Motallebi (CARB) for help assembling and checking measurements of pollutant concentrations and review of the interim report. The authors also thank Mary Tyree (UCSD), Martha Coakley (UCSD), and Josh Schriffin (UCSD) for their development of the statistical downscaling method.

Summary of Preliminary Results

The goal of this project is to identify linkages between climate and air quality for major airsheds in California. In this first interim report, a detailed perturbation analysis was carried out to study the effect of meteorology on ozone and $PM_{2.5}$ concentrations during present-day air pollution events. Two air pollution episodes in the South Coast Air Basin (SoCAB) (September 7-9, 1993; September 23-25, 1996) and one air pollution episode in the San Joaquin Valley (SJV) (January 4-6, 1996) were used to span the wide range of meteorological conditions and pollutant concentrations experienced in California. Each base-case episode has been extensively validated against measured concentrations in previous studies providing a solid foundation for the perturbation analysis.

Temperature, humidity, mixing depth, and wind speed were systematically perturbed and the corresponding change in the regional distribution of 1-hr average ozone concentrations and 24-hr average $PM_{2.5}$ concentrations was calculated. The following systematic behavior was observed across all the episodes.

1. Increased wind speed reduces ozone and $PM_{2.5}$ concentrations by enhancing dilution of primary emissions.
2. Increased mixing depth reduces $PM_{2.5}$ concentrations by enhancing dilution of primary emissions. Surface NO_X concentrations are also reduced by enhanced dilution leading to an increase in surface ozone concentrations because less NO_X is available to titrate the ozone that is produced aloft and mixed to the surface.
3. Increasing temperature with constant absolute humidity increases ozone concentrations due to increased rate of photochemical reactions but reduces $PM_{2.5}$ concentrations due to increased volatilization of ammonium nitrate and reduced particle water content.
4. Increasing temperature with constant relative humidity increases ozone concentrations further because water vapor provides a source of hydroxyl radical to the system. The additional water vapor also maintains the particle water content, reducing the volatilization of ammonium nitrate at warmer temperatures. $PM_{2.5}$ concentrations in the SoCAB decrease in response to higher temperature with constant relative humidity. The magnitude of this decrease is smaller than the case with less water vapor. Higher temperatures at constant relative humidity actually increase predicted $PM_{2.5}$ concentrations in some regions of the SJV that have cool base-case temperatures and a large excess of gas-phase ammonia.

A statistical downscaling technique was also developed to relate the frequency of meteorological conditions that encourage high ozone formation to large-scale meteorological variables predicted by GCMs. The application of this statistical downscaling technique to GFDL predictions for future climate suggests one additional conclusion.

5. Climate change will lead to higher temperatures in the troposphere. Based on statistical linkages of ozone and 850 millibar temperatures, this warming results in an increased frequency of meteorological conditions that encourage the formation

of ozone in California. The incidence of days with favorable conditions for ozone formation grows as warming increases through the 21st Century. By the end of the 21st Century, assuming the same mechanisms and base conditions prevail as today, the frequency of days with favorable conditions for ozone formation increases by 25-80%, depending on the amount of warming, which presently is not clear because of uncertainties in the sensitivity of the climate system's sensitivity to greenhouse gas emissions and the future emissions pathway that will be followed by global society.

The trends identified above suggest some preliminary conclusions about the likely effect of future climate change on air quality in California. Future temperatures during stagnation events are likely to be warmer than current temperatures, leading to the conclusion that climate change will produce meteorological conditions that favor higher ozone concentrations and a greater frequency of ozone episodes. Warmer temperatures will also favor decreased $PM_{2.5}$ concentrations in the SoCAB, and constant or slightly increased $PM_{2.5}$ concentrations in the SJV.

All of the conclusions stated above are preliminary, since meteorology is only one factor that determines air pollution in California. Changes to emissions inventories through population expansion, application of emissions control programs, interaction between future temperature and future emissions, changes to background pollutant concentrations, and changes to the frequency and duration of stagnation events must also be considered. Phase II of the current project will address some of these issues using dynamically downscaled meteorology combined with detailed air quality modeling in combination with the development of a future emissions inventory for the SJV (part of a project funded by US EPA). This more detailed analysis will support more definitive conclusions about ozone and $PM_{2.5}$ response to future climate change.

Table of Contents

1. Introduction……..1
2. Background……..4
3. Model Description for Perturbation Analysis……... 6
4. Perturbation Results for SoCAB on September 9, 1993……. 9
5. Perturbation Results for SoCAB on September 25, 1996……20
6. Perturbation Results for SJV on January 6, 1996…… 30
7. Frequency of Future Stagnation Events…… 38
8. Conclusions……. 44
9. References……47

Table of Figures

3-1 Summary of modeling domains for SJV and SoCAB……. 8

4-1 O_3 response to temperature in SoCAB on Sept 9, 1993…….. 14
4-2 $PM_{2.5}$ response to temperature in SoCAB on Sept 9, 1993……. 15
4-3 O_3 response to temperature at constant RH in SoCAB on Sept 9, 1993……. 16
4-4 $PM_{2.5}$ response to temperature at constant RH in SoCAB on Sept 9, 1993…… 17
4-5 O_3 response to mixing depth and wind speed in SoCAB on Sept 9, 1993…….. 18
4-6 O_3 response to mixing depth and wind speed in SoCAB on Sept 9, 1993…….. 19

5-1 O_3 response to temperature in SoCAB on Sept 25, 1996…… 24
5-2 $PM_{2.5}$ response to temperature in SoCAB on Sept 25, 1996…….. 25
5-3 O_3 response to temperature at constant RH in SoCAB on Sept 25, 1996…….. 26
5-4 $PM_{2.5}$ response to temperature at constant RH in SoCAB on Sept 25, 1996….. 27
5-5 O_3 response to mixing depth and wind speed in SoCAB on Sept 25, 1996…… 28
5-6 O_3 response to mixing depth and wind speed in SoCAB on Sept 25, 1996…… 29

6-1 O_3 and $PM_{2.5}$ response to temperature in SJV on Jan 6, 1996…… 35
6-2 O_3 and $PM_{2.5}$ response to temperature at constant RH in SJV on Jan 6, 1996… 36
6-3 O_3 and $PM_{2.5}$ response to mixing depth in SJV on Jan 6, 1996…….. 37

7-1 Count of days with O_3 > 90 ppb vs. monthly-average T850…….. 41
7-2 Predicted SoCAB days per year with O_3 > 90 ppb assuming constant emissions42
7-3 Predicted SJV days per year with O_3 > 90 ppb assuming constant emissions… 42
7-4 Predicted SoCAB fall days per year with precipitation > 0.02mm……43
7-5 Predicted SJV winter days per year with precipitation > 0.02mm……..43

8-1 Summary of O_3 and $PM_{2.5}$ response to meteorological variables in CA……46

1. Introduction

California's unique combination of large urban populations situated in confined air basins that are subject to severe air pollution events causes significant public health concerns. Ozone and airborne particulate matter are two of the main ingredients of the photochemical "smog" that can form when atmospheric mixing is low, causing pollutants to be trapped near the earth's surface. The adverse health effects of ozone and airborne particulate matter are widely acknowledged, and reducing the concentrations of these pollutants is an important objective for the State of California.

Meteorological patterns that encourage the formation of stagnation events play a significant role in the determination of air pollution concentrations in California. Measurements show that annual variability in temperature and precipitation has a large effect on ozone and $PM_{2.5}$ concentrations. Large scale meteorological patterns such as El Niño events may persist for 1 year, returning every 3-7 years, can significantly change the frequency and severity of air pollution episodes. The persistence of La Niña and El Niño events—which cause abnormal sea-surface temperatures thereby affecting worldwide weather patterns— might be part of a larger, long-lasting climate pattern.

El Niño conditions existed during 1997 and 1998, followed by La Niña conditions during 1999. Both conditions may have impacted ozone formation during this period. In southern California, during the four-month SCOS97-NARSTO field study, the peak ozone concentration observed over all of the 13 Intensive Operation Period days was 19 pphm. Ozone concentrations and photochemical activity were unusually low by comparison to past years in the South Coast Air Basin (SoCAB) throughout the entire study period. An increased frequency of positive vorticity advection and mid-atmospheric troughing just west of the Pacific Coast (associated with El Niño activity) is thought to have contributed to a deeper marine layer and better mixing than usual over the SoCAB during the summer and early fall of 1997. Similar pollution trends were observed in the San Joaquin Valley (SJV) during the El Niño event of 1997. Only thirty six days had 1hr-average ozone concentrations greater than 90ppb at Visalia (in the SJV) during 1997 compared to sixty nine days the year before.

In contrast to El Niño and La Niña events that last for 1 year, climate change refers to a sustained shift in meteorological patterns that gradually occurs over a longer time period. It is expected that climate change will significantly affect meteorological patterns in California over the next decade and longer. The implications of climate change on air quality problems in California are largely unknown.

The first step towards an understanding of how future climate will affect future air quality is to understand how present-day climate affects present-day air quality. The most direct route towards this understanding is a systematic perturbation study where one meteorological variable is changed at a time and the resulting change in air quality is calculated. These perturbation studies should be carried out for each of the characteristic types of air pollution episodes that occur in California.

The first major objective of this interim report is to present the results from a perturbation analysis for the air pollution episodes that occurred in the South Coast Air Basin (SoCAB) on September 7-9, 1993, in the SoCAB on September 23-25, 1996, and in the San Joaquin Valley (SJV) on January 4-6, 1996. The SoCAB and the SJV are the two most heavily polluted air basins in California. The air pollution episodes described above are distinctly different in character but each episode has ozone and/or $PM_{2.5}$ concentrations that greatly exceed the standards designed to protect human health. The extensive meteorological, emissions, and air quality information needed to support detailed modeling of each episode has been assembled previously, and base-case modeling studies have validated the performance of air quality models used to simulate the formation of pollutant concentrations. Table 1 summarizes the focus pollutants used in each episode and the published studies describing those episodes.

Temperature, relative humidity, mixing depth, and wind speed were uniformly perturbed by an amount that is representative of expected changes due to climate variation. The response of ozone and $PM_{2.5}$ concentrations that is induced by each perturbation was calculated, and common patterns of behavior across multiple air basins and episodes were be identified.

Table 1: Air quality episodes to be studied with sensitivity analysis.

		Location	
		SoCAB	SJV
Focus Pollutant	O_3	Date: September 7-9, 1993 References: [1, 2]	Footnote a.
	PM	Date: September 23-25, 1996 References: [3-5]	Date: January 3-5, 1996 References: [6]

a. Sensitivity analysis of ozone response to climate change in the SJV is being conducted as part of a separate project funded by the US EPA at UC Berkeley. The results of this analysis will be published and made available for the current project as soon as possible, but they may not be available before the end of 2005.

The results from the expanded perturbation analysis described above have been combined with the results from previous research to produce an overall evaluation of the effect of meteorology on air pollution in California. This combination of current and previous research was necessary to meet the aggressive timeline for the current project. Sections of the current report have been extracted from the following previously published material:

M.J. Kleeman, “Assessing Changes in PM2.5 Due to Changes in Temperature”, Final Report for the U.S. Environmental Protection Agency Contract # R-82824201-01.

J. Aw and M.J. Kleeman, “Evaluating the First-Order Effect of Intra-annual Temperature Variability on Urban Air Pollution”, Journal of Geophysical Research-Atmospheres (108) D12, 2003.

M.J. Kleeman and G.R. Cass, "A 3D Eulerian source-oriented model for an externally mixed aerosol", Environmental Science and Technology (35) 4834-4848, 2001.

A.E. Held, Q. Ying, A. Kaduwela, and M.J. Kleeman "Modeling particulate matter in the San Joaquin Valley with a source-oriented externally mixed three-dimensional photochemical grid model", Atmospheric Environment (38), 3689-3711, (2004).

M.J. Kleeman, Q. Ying, and A. Kaduwela, "Control Strategies for the reduction of airborne particulate nitrate in California's San Joaquin Valley". Atmospheric Environment in press (2005).

All of the results from model simulations presented in the following chapters were produced specifically for the current report. The methodology used to produce these model results is partly described in the references listed above. Further updates were also made to the secondary organic aerosol (SOA) formation mechanism that was used for SoCAB simulations in this report as part of a collaboration with an ongoing US EPA project. The SOA formation mechanism was not updated for simulation of the winter SJV episode because the low photochemical activity during this episode is expected to produce minimal amounts of SOA.

The second major objective of this interim report is to describe the development of a statistical downscaling technique that can predict the frequency of meteorological events that encourage the formation of air pollution in California. The statistical downscaling technique was applied to GCM predictions through the year 2100 to predict how climate change will contribute to the frequency of air pollution episodes in California.

2. Background

Scientists at University of California, Los Angeles, have modeled the effects of climate change on parameters such as precipitation, snowpack, forest cover, and stream flow, but not air quality or human exposure [7-9]. They showed a strong increase in heat waves and extreme heat in Los Angeles and greater increases in summer temperatures as compared with winter temperatures, supporting the hypothesis of higher temperatures during the smog season (May to October) under future climate scenarios.

Previous studies have examined the effect of climate on regional air quality in the central and eastern portions of the United States [10]. These studies used output from Global Climate Models (GCMs) to study the frequency of large scale weather patterns that promote the formation of air pollution events. The GCM output can also be dynamically downscaled using regional meteorological models to simulate air pollution formation with regional air quality models. The results of these previous studies predict that the frequency of summer ozone air pollution events will increase in the future due to altered climate and increased background concentrations of ozone.

A directed study of the eastern U.S. [11] found that, around 2050, climate change would be the most important factor leading to increases in the upper quartile of 8-hour average surface ozone concentrations, whereas projected changes in anthropogenic emissions would cause increases only half as large. Moreover, estimated changes in surface conditions (e.g., vegetation cover) would have the least effect on the upper quartile of 8-hr ozone abundances. Similar conclusions were reached by Langner et al. [12] regarding future surface ozone concentrations in Europe. This research strongly suggests changing climate will be the primary driver of variations in surface ozone by 2050. Nevertheless, substantial contributions associated with changes in emissions (and surface conditions) should also be taken into account.

The analysis of climate change on regional particulate matter concentrations is less certain because air quality models for particulate matter are more complex and computationally challenging than ozone models. Sensitivity studies have been carried out to examine how regional particulate air pollution responds to direct changes in temperature, relative humidity, and mixing depth during a typical air pollution episode that occurred in SoCAB [13]. The results of this analysis suggested that increased temperature increases ozone concentration and the production of semi-volatile secondary products, but reduces the partitioning of those semi-volatile products to the particle phase.

A new aspect of the long-term concern about exposure to air pollution, and the public health consequences of that exposure, is potential impact of changes in Earth's climate associated with emissions of greenhouse gases leading to global warming. It is well known that atmospheric conditions affect photochemical smog formation, as well as emissions from vehicular and stationary sources of volatile organic compounds and oxides of nitrogen. However, while such phenomena have been studied extensively for

present climatic conditions, there is an urgent need to project air quality and exposure levels for future climate change scenarios by performing a more comprehensive analysis of the effect of climate change on air quality in California.

3. Model Description For Perturbation Analysis

Figure 3-1 illustrates the air quality modeling domains used to represent the SJV and the SoCAB in the current study. The SJV modeling region is a 54 x 72 rectangular domain with a grid size of 4km using the Lambert coordinate system. The SoCAB modeling region is an 80 x 30 rectangular domain with a grid size of 5 km using the UTM coordinate system. The SJV domain uses five vertical layers with depth of 38.5, 115.5, 154, 363 and 429 meters (which gives a total high of 1100 meters in the vertical). The SoCAB domain applied to the September 7-9, 1993 episode uses the same vertical structure. The SoCAB domain applied to the September 23-25, 1996 episode used 7 vertical layers with depths 35, 65, 100, 200, 200, 200, and 200 for a total depth of 1000m. The ~1km model depth is sufficient to resolve air pollution episodes in California since they occur in well defined air basins in the presence of temperature inversions at elevations of 0-700m.

The internally-mixed version of the UCD-CIT air quality model was used to predict the response of pollutant concentrations to changes in meteorological parameters. Previous studies [4-6, 14] have described the formulation of the UCD/CIT source-oriented air quality model, and so only those aspects that differ for the current project are discussed here.

SJV

The gas-phase chemical mechanism used to model episodes in the SJV is based on the SAPRC90 [15] mechanism with extensions to predict the formation of 10 semi-volatile organic compounds [16]. The partitioning of semi-volatile organic species to the particle phase is calculated using an absorption model calibrated using surrogate species that have representative properties for the 10 lumped model compounds [17]. The temperature dependance of the surrogate species is estimated using the Classius Clapyron equation based on a literature survey of available thermodynamic data [13]. Photochemical activity in the SJV is low during the winter months when airborne particulate matter episodes occur, leading to low predictions for SOA concentrations.

SoCAB

The gas-phase mechanism used to model episodes in the SoCAB is the Caltech Atmospheric Chemistry Model (CACM) [18, 19]. The thermodynamic data describing the partitioning of semi-volatile reaction products between the gas phase, condensed organic phase, and condensed aqueous phase [19, 20] were adapted to work with the UCD/CIT air quality model. Ethane was removed from the lumped model species ALKL and tracked as an individual species so that a more appropriate rate constant could be specified for reaction with hydroxyl radical. The model subroutines that partition inorganic and organic species between the gas and particle phases were combined so that the inorganic and organic mechanisms could be more tightly coupled. The new routines simultaneously predict the vapor pressure of semi-volatile inorganic and organic species above each particle by calculating the thermodynamic equilibrium concentration for each

species between a solid (inorganic species only), organic (organic species only) and aqueous (inorganic and organic species) phase. Activity coefficients for inorganic species are calculated using the method described by Kusik and Meissner [21]. Activity coefficients for organic species are calculated using the UNIFAC model [22]. Experimental data describing interactions between organic and inorganic species is sparse [23, 24] and so these interactions are neglected in the current study. Likewise, heterogeneous acid-catalyzed reactions leading to the formation of low-volatility organic compounds have been observed in several studies [25-27] but a comprehensive representation of these reactions suitable for use in an air quality model have not yet been formulated. In the current study, the general effect of acid catalyzed reactions is accounted for by adjusting the vapor pressures of surrogate compounds used to represent the semi-volatile organic species as discussed by Griffin et al. [19]. This procedure is applied to all particles without considering their chemical composition.

Both inorganic and organic species in the aqueous phase are used to calculate the partial vapor pressure of water above the particle surface. The exchange of all semi-volatile species (including water) between the gas phase and particles is calculated as a dynamic process using equations described by Kleeman et al. [28]. At low relative humidity, when aerosol water content becomes so small that some particles become solid, the volume available for aqueous organic species to partition into becomes negligible, reducing aqueous organic concentrations to zero. Under these conditions, the only semi-volatile species contained on particles are solid inorganic species and SOA in the condensed organic phase. Dry particles can spontaneously form a new aqueous phase when relative humidity increases.

Perturbations

Temperature perturbations to be considered in the present study include +2 K and +5 K. These values span the range of IPCC projections for global mean surface temperature rise over the next 100 years. The actual temperature rise in California is not uniform and it may differ from these values. Never-the-less, +2 K and +5 K perturbations provide a useful starting point to investigate sensitivity.

Humidity perturbations to be considered in the present study are combined with temperature perturbations to avoid artificially specifying an atmosphere with RH>100%. Each temperature perturbation will be evaluated once with constant absolute humidity and once with constant relative humidity. The likely change in humidity will occur somewhere between these limiting cases.

Perturbations in wind speed and mixing depth considered in this study were arbitrarily chosen to be +20% and +50%, respectively. These values should result in an observable effect, enabling some evaluation of the sensitivity of pollutant concentrations to these variables.

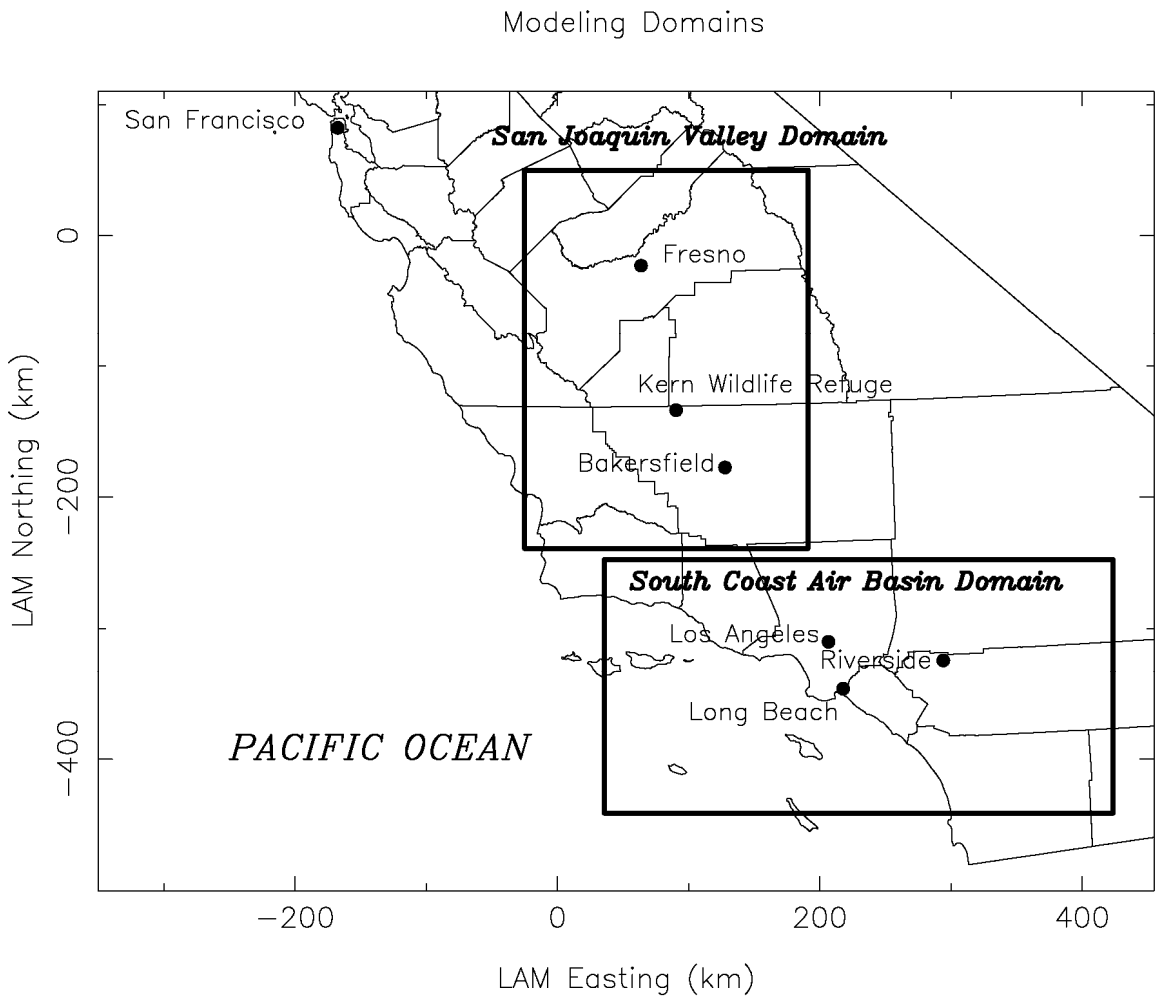

Figure 3-1: Modeling domains used for sensitivity studies in the San Joaquin Valley and the South Coast Air Basin [14].

4. Perturbation Results for Southern California on September 9, 1993

Meteorological Patterns [29]

The SoCAB is California's largest metropolitan region, which covers an area of approximately 16,700 km^2. It is bounded on the north by the San Gabriel and San Bernardino Mountains, on the east by the San Jacinto Mountains, and on the west and south by the Pacific Ocean. Elevated particulate matter concentrations usually occur in the spring and fall when photochemical reaction rates are large but temperatures are still relatively cool. Analysis indicates that the prevailing wind direction during these seasons is from the west and south over the Pacific Ocean to the inland region during the morning, switching to predominantly westerly winds by the afternoon. Intensive dairy operations in the east end of the SoCAB release large amounts of ammonia that combines with the nitric acid formed from photochemical reactions to produce high concentrations of secondary ammonium nitrate.

The severe air quality episode that occurred in the SoCAB during the period September 7-9, 1993 was characterized by daytime surface temperatures exceeding 35°C at inland locations and a strong elevated temperature inversion. Light surface winds followed the land-sea breeze pattern with onshore flow during the day and stangation at night. Upper level winds originated from the north – north west of the modeling domain (over land), perhaps contributing to the hot daytime temperatures. This episode producted extreme ozone concentrations, even by current SoCAB standards.

Model Application

The preparation of meteorological and emissions input data needed for photochemical modeling of this episode has been described previously [1, 2] and so only a brief summary is provided here. Surface meteorological parameters were measured at 50 sites in the model region operated by the California Irrigation Management System, the South Coast Air Quality Management District, and the National Climatic Data Center. Elevated meteorological parameters were measured at West Los Angeles by the South Coast Air Quality Management District and at Claremont by the California Air Resources Board. The meteorological measurements were interpolated using a diagnostic meteorology model [30] to produce continuous meteorological fields with hourly resolution needed by the air quality simulation.

Emissions information was provided by the SCAQMD based on the emissions inventories used to support the 1997 Air Quality Management Plan along with temperature corrections for evaporative emissions based on the temperature conditions experienced on September 7-9, 1993. The emissions from the Los Angeles International Airport were updated in the current work based on the inventory developed for the summer 1997 Southern California Ozone Study (SCOS97). Biogenic emissions were represented using the biogenic inventory developed for the late August 1987 episode of the Southern California Air Quality Study (SCAQS) with appropriate temperature corrections for the conditions experienced on September 7-9, 1993. Particle-phase

emissions were speciated using measured emissions profiles [31-37] and then combined into 9 inorganic model species and 9 lumped carbonaceous model species based on chemical structure (normal alkanes, polycyclic aromatic hydrocarbons (PAH), oxygenated PAH, diacids, aliphatic acids, substituted monoaromatic compounds, cyclic petroleum biomarkers, "other organic compounds", and elemental carbon). The size distribution of particulate matter emissions from different sources was specified in 15 sections spanning 0.01 – 10 µm particle diameter based on source emission measurements [38-40]. Gas-phase organic emissions were speciated using measured emissions profiles [33-37, 41] and then combined into 24 lumped model organic species [18] based on chemical structure, reactivity, and experimentally determined SOA formation potential.

Results

Measured ozone concentrations in the SoCAB on September 9, 1993 exceeded 250 ppb, while 3-hr average $PM_{2.5}$ concentrations reached a maximum value of 90 µg m^{-3}. Model predictions have been compared to measured concentrations with good agreement [29].

Figure 4-1 (a) shows the predicted regional pattern of 1hr-average ozone concentrations on September 9, 1993 at 1500 PST. A band of high ozone concentrations is predicted to occur alone a line connecting Claremont, Riverside, and Perris, with the highest predicted concentrations reaching 290 ppb at Perris. Regional concentrations of ozone over the entire modeling domain are large during the episode, approaching 90 ppb. Predicted ozone concentrations in the region immediately downwind of Central Los Angeles are slightly lower than the regional average because they are suppressed by emissions of fresh NO_X.

Figure 4-1(b) shows the predicted increase in regional ozone concentrations at 1500 PST on September 9, 1993 when temperature is uniformly perturbed by +2 K at all times and locations. Ozone concentrations along the line connecting Claremont, Riverside, and Perris increase by approximatley 18 ppb in response to this change. Regional ozone concentrations at other locations increase by 4-5 ppb. Small regions with a ~1 ppb decrease are also observed, but these effects are minor compared to increases at other locations.

Figure 4-1(c) shows the predicted increase in regional ozone concentrations at 1500 PST on September 9, 1993 when temperature is uniformly perturbed by +5 K at all times and locations. Ozone concentrations along the line connecting Claremont, Riverside, and Perris increase by approximatley 40 ppb in response to this change. Regional ozone concentrations at other locations increase by 12-14 ppb. Small regions with a ~3 ppb decrease are also observed, but these effects are minor compared to increases at other locations.

Figure 4-2(a) shows the predicted regional pattern of 24-hr average $PM_{2.5}$ concentrations on September 9, 1993. The largest $PM_{2.5}$ concentrations 194 µg m^{-3} are predicted to occur in the region west of Riverside where ammonia concentrations are very large leading to enhanced formation of particulate ammonium nitrate. The predicted

concentration of $PM_{2.5}$ at most other locations in the inland portion of the modeling domain is 70-90 μg m^{-3}. Hotter temperatures suppress the formation of particulate nitrate [13]. The hot base-case temperatures during the current episode suppress the formation of large regions of particulate nitrate.

Figure 4-2(b) shows the predicted change in regional $PM_{2.5}$ concentrations on September, 1993 when temperature is uniformly perturbed by +2 K at all times and locations. $PM_{2.5}$ concentrations in the region east of Riverside decrease by 14 μg m^{-3} in response to this change. The majority of this reduction is associated with the volatilzation of particulate ammonium nitrate as temperature increases. The location west of Riverside with the highest base-case concentration of particulate nitrate (see Figure 4-2(a)) does not experience the largest reduction in $PM_{2.5}$ concentrations because regions with higher excess gas-phase ammonia concentrations respond less strongly to increased temperature than regions with lower excess gas-phase ammonia [13]. Figure 4-2(b) also shows that regional average $PM_{2.5}$ concentrations are predicted to decrease by 3-5 μg m^{-3} in response to the +2 K temperature perturbation. Once again, this change is caused by the partitioning of semi-volatile species to the gas phase at hotter temperatures, with particulate ammonium nitrate being the largest contributor to this effect. The region around the Long Beach harbor experiences a 0.2 μg m^{-3} increase in $PM_{2.5}$ concentrations in response to a +2 K temperature perturbation. Increased temperature promotes the oxidation of SO_2 emissions in this region to form sulfuric acid. Sulfur acid is essentially non-volatile at all ambient temperatures, and so this species partitions to the particle phase regardless of temperature perturbation.

Figure 4-2(c) shows the predicted change in regional $PM_{2.5}$ concentrations on September 9, 1993 when temperature is uniformly perturbed by +5 K at all times and locations. The change in regional $PM_{2.5}$ concentrations in this case is very similar to the trends shown in Figure 4-2(b), but additional ammonium nitrate evaporates in the region east of Riverside, leading to a maxium decrease in $PM_{2.5}$ concentrations of 31 μg m^{-3}.

Figure 4-3(b) shows the change in predicted regional ozone concentrations at 1500 PST on September 9, 1993 when temperature is uniformly perturbed by +2 K while relative humidity is held constant. This figure can be compared to Figure 4-1(b) which applied a +2 K temperature perturbation while absolute relative humidity was held constant. The spatial distribution of increased ozone concentrations shown in Figure 4-3(b) matches that shown in Figure 4-1(b), but the magnitude of the predicted concentration increase is 30 ppb (vs. 18 ppb for the case with lower humidity). Water vapor is a source of hydroxyl radicals in urban areas, and so the increased humidity increases the reactivity of the atmosphere.

Figure 4-3(c) shows the change in predicted regional ozone concentrations at 1500 PST on September 9, 1993 when temperature is uniformly perturbed by +5 K while relative humidity is held constant. This figure can be compared to Figure 4-1(c) which applied a +5 K temperature perturbation while absolute relative humidity was held constant. Once again, the spatial pattern of the increased ozone concentration is similar, but the magnitude of the concentrations increase is enhanced by the addition of water vapor to

the system. The maximum change in ozone concentration under this condition is 67 ppb (vs. 40 ppb for the case with lower humidity).

Figure 4-4(b) shows the change in predicted regional $PM_{2.5}$ concentrations on September 9, 1993 when temperature is uniformly perturbed by +2 K while relative humidity is held constant. This figure can be compared to Figure 4-2(b) which applied a +2 K temperature perturbation while absolute humidity was held constant. Increased humidity will increase the amount of particle-phase water, leading to enhanced partitioning of soluble semi-volatile species. This effect partly counteracts the effect of increased temperature during this perturbation, which tends to force more semi-volatile material into the gas phase. The region immediate west of Riverside experiences no decrease in $PM_{2.5}$ concentrations when temperature is increased by +2 K with constant relative humdity, and one grid cell (4km x 4km area) even experiences a 2 $\mu g\ m^{-3}$ increase $PM_{2.5}$ concentrations. The area east of Riverside still experiences a decrease of $PM_{2.5}$ concentrations by approximately 7 $\mu g\ m^{-3}$, but this is reduced from the decrease of 14 $\mu g\ m^{-3}$ predicted in the case with lower humidity. The regional average $PM_{2.5}$ concentrations also show reduced response to a +2 K increase in temperature when relative humidity remains constant. Most inland regions experience a decrease in predicted $PM_{2.5}$ concentrations of 1-3 $\mu g\ m^{-3}$, with slight increases predicted in the region around the Long Beach Harbor, and the Los Angeles International Airport. The regional increases in $PM_{2.5}$ at these locations are once again associated with the enhanced production of sulfate aerosol from SO_2 emissions.

Figure 4-4(c) shows the change in predicted regional $PM_{2.5}$ concentrations on September 9, 1993 when temperature is uniformly perturbed by +5 K while relative humidity is held constant. This figure can be compared to Figure 4-2(c) which applied a +5 K temperature perturbation while absolute humidity was held constant. The trends shown in Figure 4-4(c) match the results shown in Figure 4-4(b). Peak concentrations in the region with extremely high gas-phase ammonia concentrations increase slightly in response to the temperature perturbation. Likewise, cooler coastal locations with moderate SO_2 emissions experience an increase in predicted $PM_{2.5}$ concentrations. The reduction of ammonium nitrate in other regions as temperature increases is mitigated by the effect of increased humidity. The largest reduction in $PM_{2.5}$ concentrations in response to the +5 K temperature perturbation with constant humidity is 19 $\mu g\ m^{-3}$ (vs. 31 $\mu g\ m^{-3}$ for the case with reduced humidity).

Figure 4-5(b) shows the change in predicted regional ozone concentrations at 1500 PST on September 9, 1993 in response to a uniform increase in mixing depths of +50%. The increased mixing depths increase predicted ozone concentrations in the western portion of the model domain by 75 ppb and decrease predicted ozone concentrations in the eastern portion of the model domain by 36 ppb. The location of the maximum concentration increase differs slightly from the location of the predicted ozone maxium in the base-case simulation, and so the net effect of the increased mixing depth is to slightly increase the maxium ozone concentrations predicted during the episode and to increase the size of the region experiencing those maximum concentrations. The observation that mixing depth increases ozone concentrations during severe photochemical episodes in the

SoCAB has been noted previously during simulations of the Southern California Air Quality Study (SCAQS).

Figure 4-5(c) shows the change in predicted regional ozone concentrations at 1500 PST on September 9, 1993 in response to a uniform increase in wind speed of +20%. Perturbed wind fields were produced by increasing the measured wind speed values that are used by the diagnostic meteorological model to generate continuous divergence-free wind fields. Increased wind speed reduces the concentration of pollutant emisions in ground-level cells and moves high concentration plumes to different locations. The results shown in Figure 4-5(c) show that predicted ozone concentrations in the wester portion of the model domain increase by 8 ppb in response to increased wind speeds, but the maximum predicted concentrations along the line connecting Claremont, Riverside, and Perris are decreased by 107 ppb. The net effect of the increased wind speeds is to make the predicted ozone concentrations more uniform across the model region, with an overall reduction in peak ozone concentrations during the current episode.

Figure 4-6(b) shows the change in predicted regional $PM_{2.5}$ concentrations on September 9, 1993 in response to a uniform increase in mixing depth of +50%. The maximum increase in $PM_{2.5}$ concentrations in response to this change is 5 $\mu g\ m^{-3}$ in the region that experienced the largest increase in ozone concentrations (see Figure 4-5(b)). Predicted $PM_{2.5}$ concentrations in the region to the east of Riverside are reduced by 9 $\mu g\ m^{-3}$ as the plume of enhanced nitrate is diluted by the increased mixing depth.

Figure 4-6(c) shows the change in predicted regional $PM_{2.5}$ concentrations on September 9, 1993 in response to a uniform increase in wind speed of +20%. Small increases of ~2 $\mu g\ m^{-3}$ $PM_{2.5}$ are predicted in a few locations, but the major change associated with this perturbation is a predicted reduction of 44 $\mu g\ m^{-3}$ in $PM_{2.5}$ concentrations at the location of maximum base-case $PM_{2.5}$. The majority of this effect is likely associated with reduced ammonia concentrations in the regions near the agricultural sources to the west of Riverside.

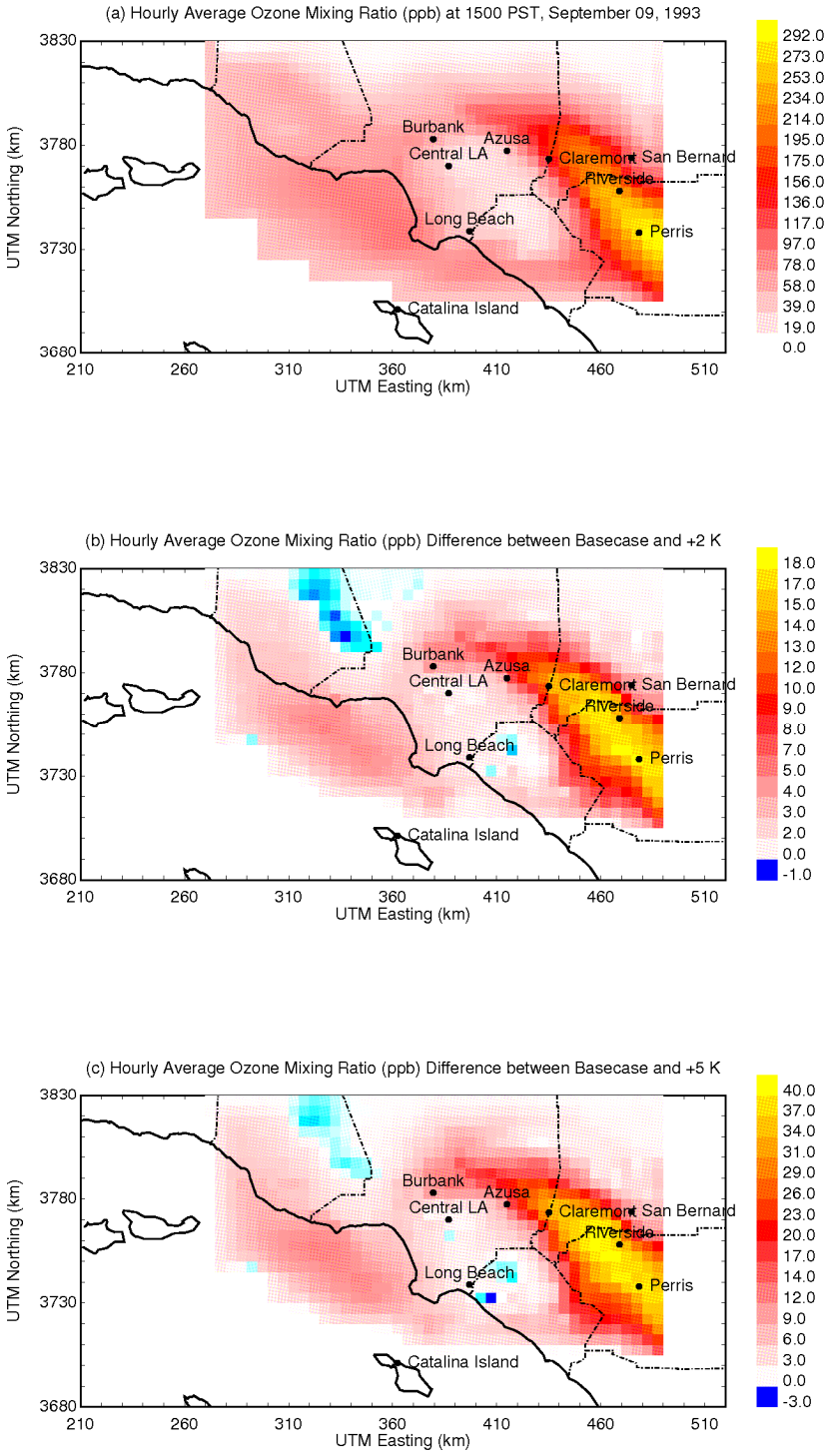

Figure 4-1: Hourly average ozone mixing ratio (panel a) and ozone mixing ratio difference in response to uniform temperature perturbations (panels b,c) at 1500 PST on September 9, 1993. Units are ppb.

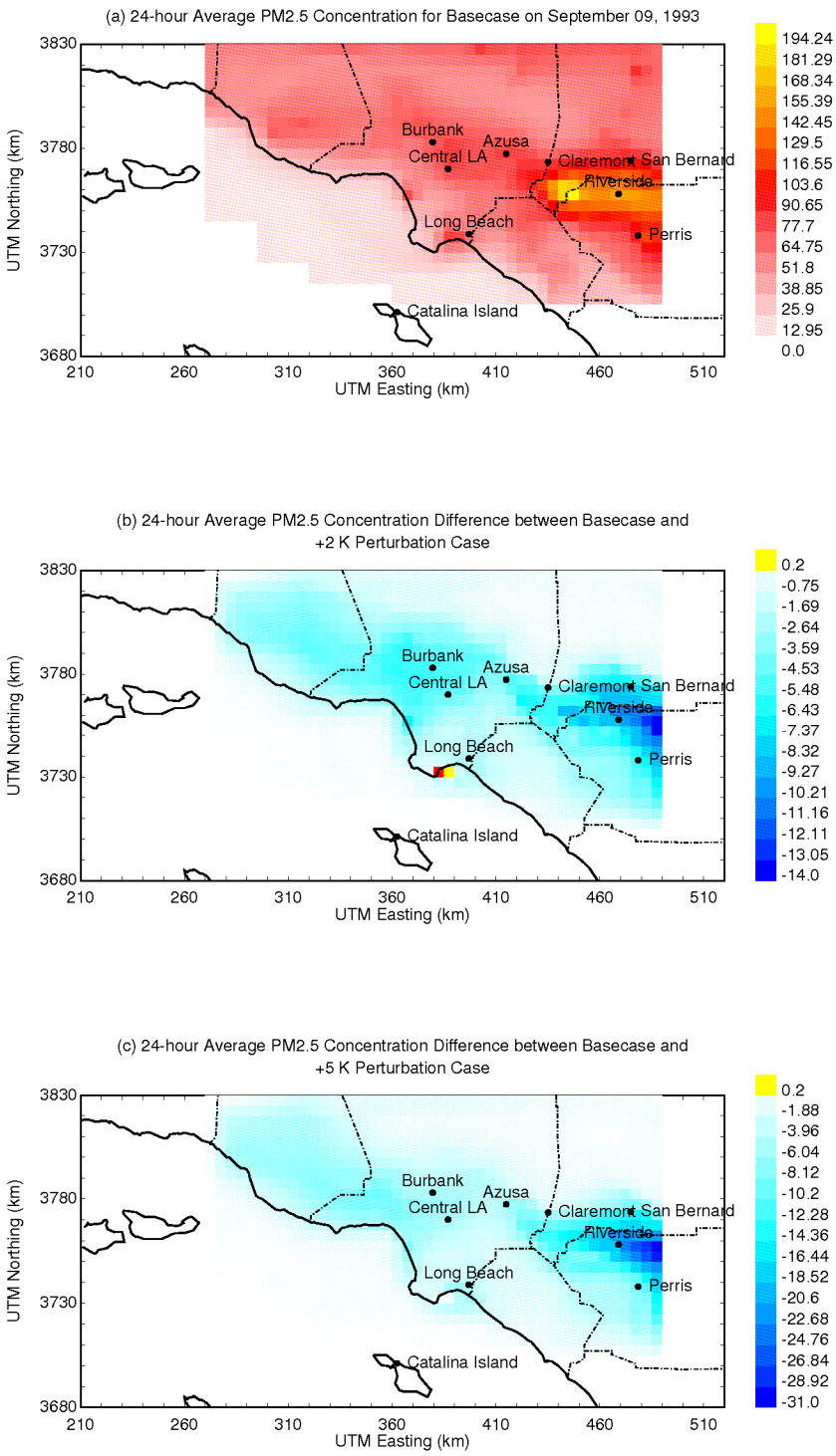

Figure 4-2: 24-hr average $PM_{2.5}$ concentration (panel a) and 24-hr average $PM_{2.5}$ concentration difference in response to uniform temperature perturbations (panels b,c) on September 9, 1993. Units are $\mu g\ m^{-3}$.

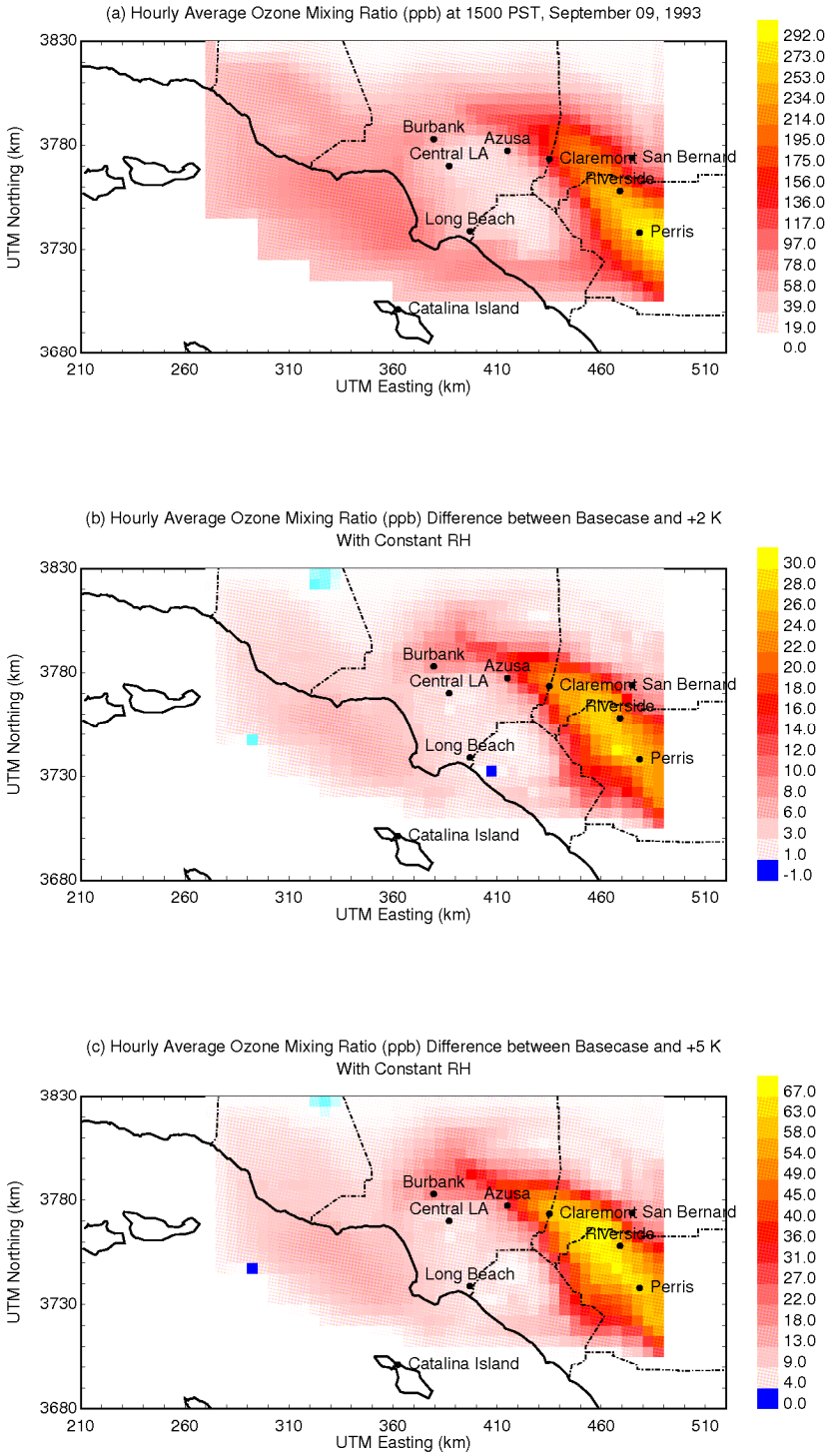

Figure 4-3: Hourly average ozone mixing ratio (panel a) and ozone mixing ratio difference in response to uniform temperature perturbations with constant relative humidity (panels b,c) at 1500 PST on September 9, 1993. Units are ppb.

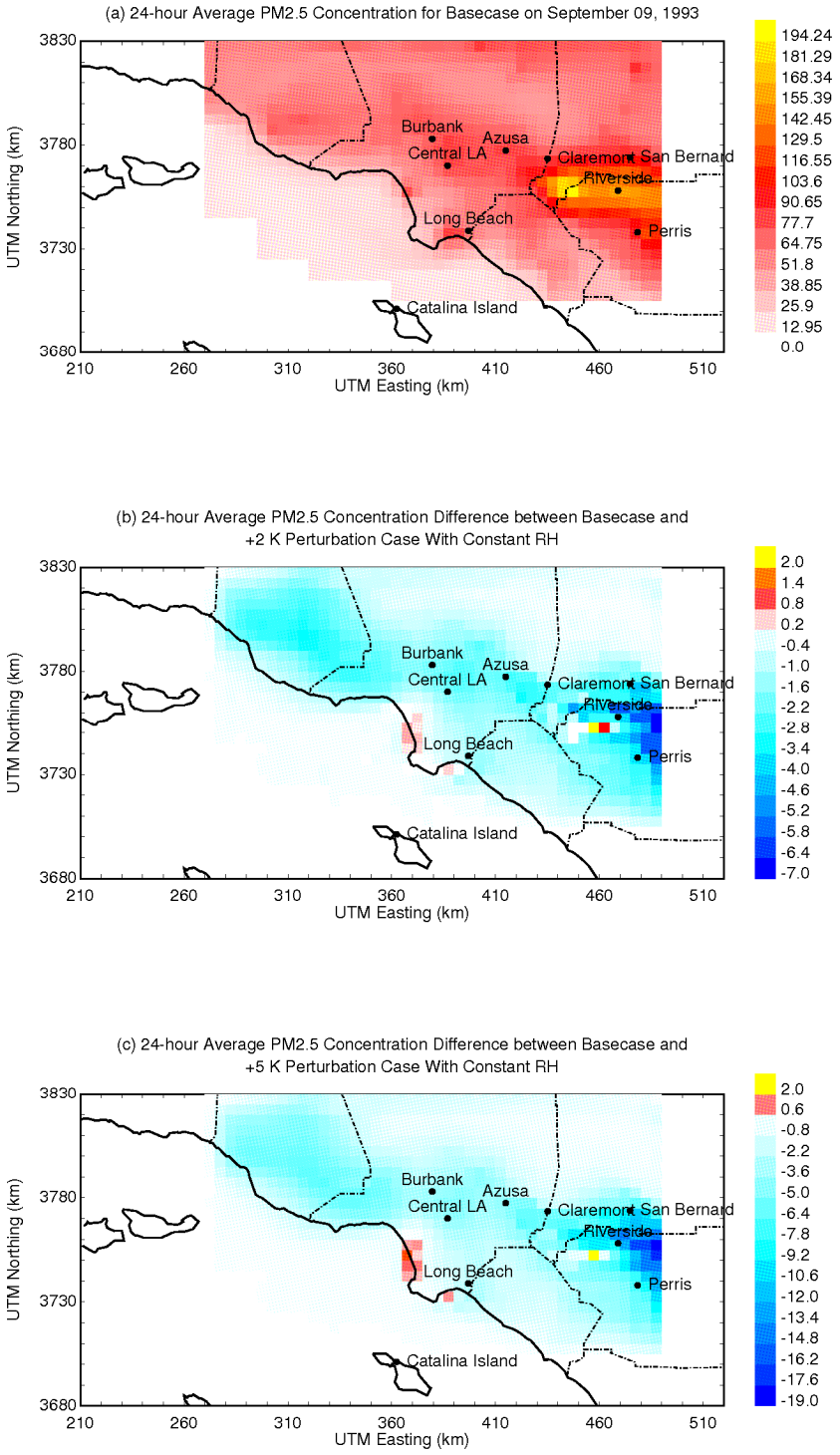

Figure 4-4: 24-hr average $PM_{2.5}$ concentration (panel a) and 24-hr average $PM_{2.5}$ concentration difference in response to uniform temperature perturbations with constant relative humidity (panels b,c) on September 9, 1993. Units are µg m-3.

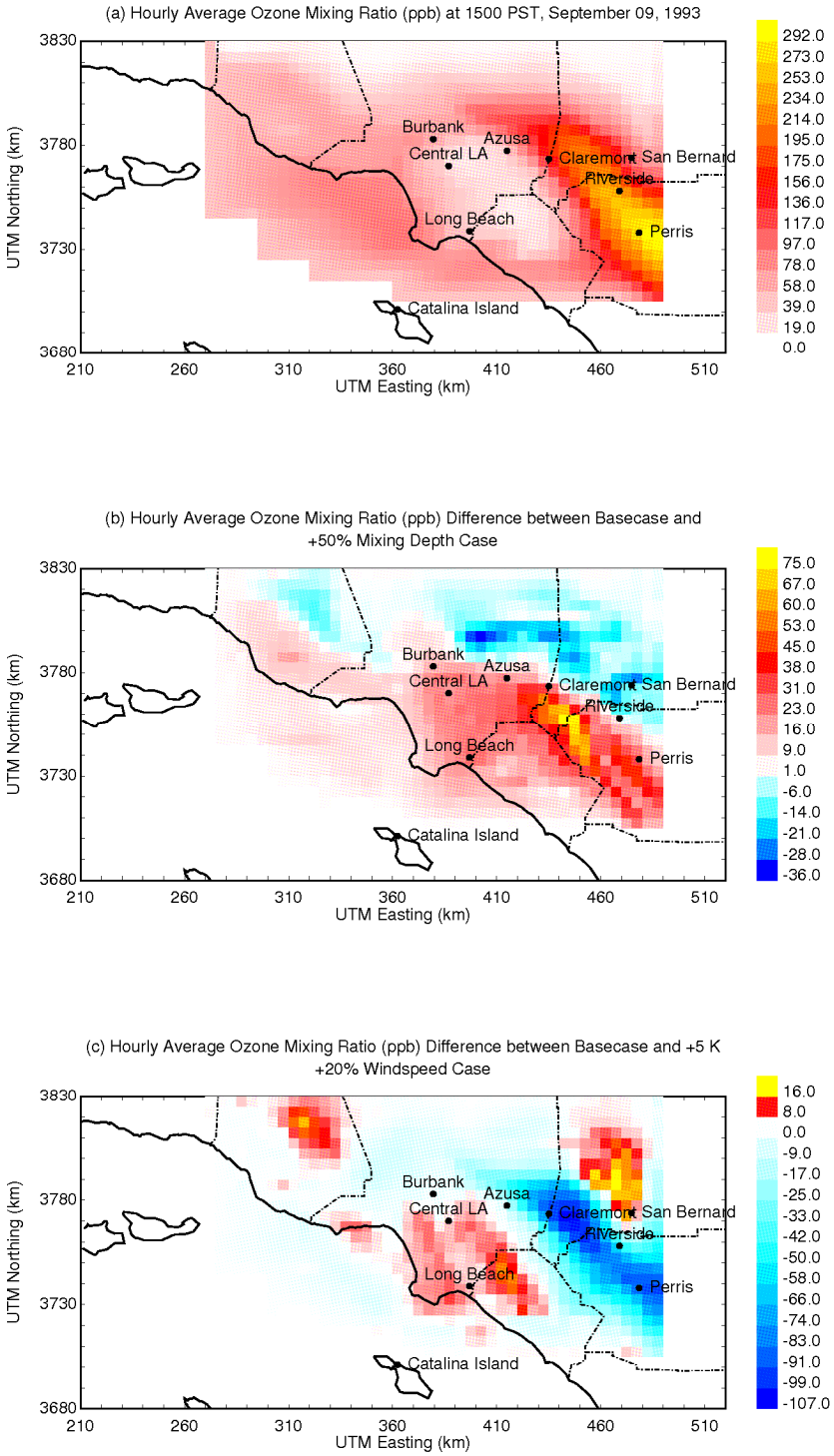

Figure 4-5: Hourly average ozone mixing ratio (panel a) and ozone mixing ratio difference in response to +50% increase in mixing depth (panels b) and +20% increase in wind speed (panel c) at 1500 PST on September 9, 1993. Units are ppb.

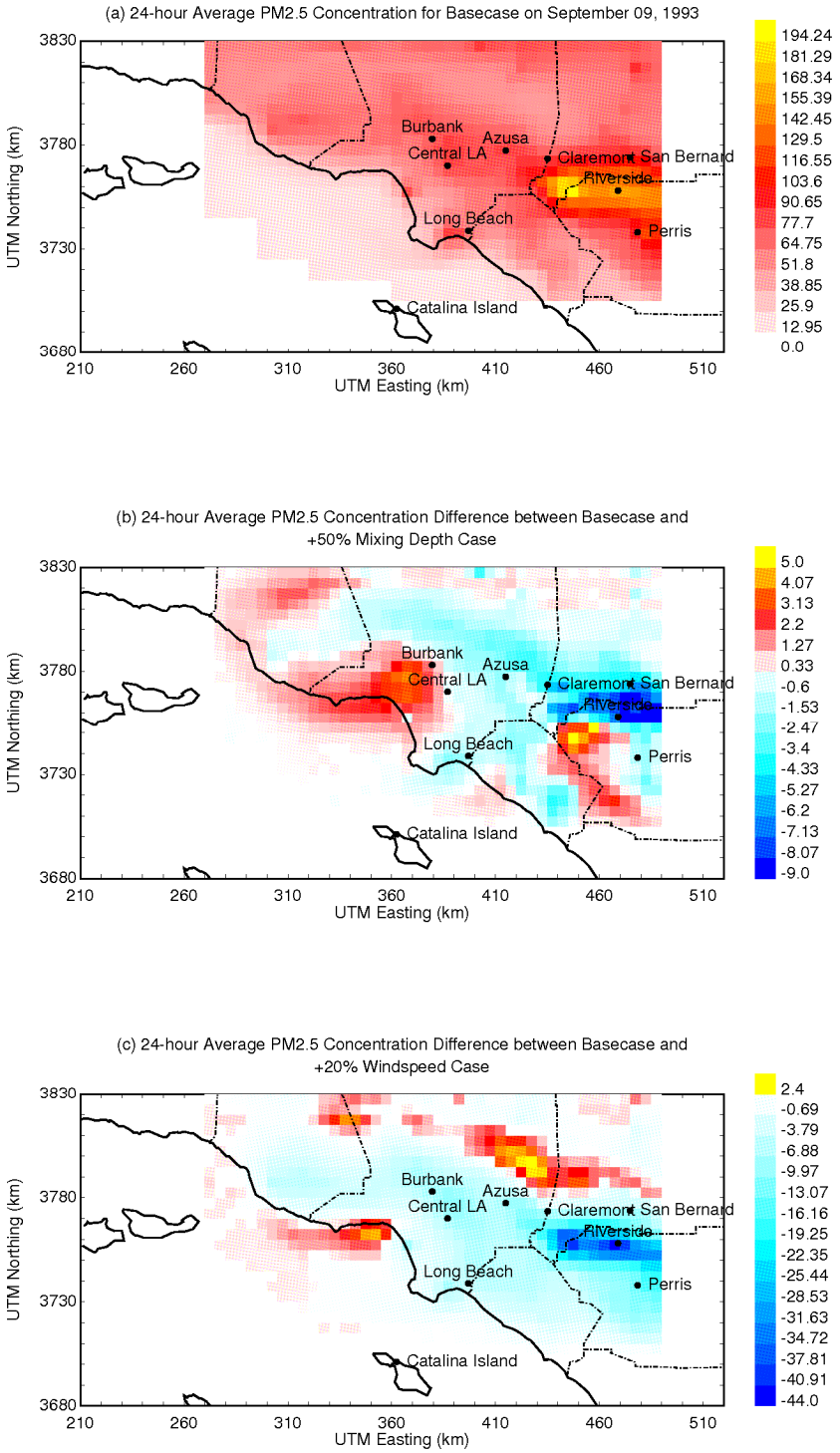

Figure 4-6: 24-hr average $PM_{2.5}$ concentration (panel a) and 24-hr average $PM_{2.5}$ concentration difference in response to +50% increase in mixing depth (panels b) and +20% increase in wind speed (panel c) on September 9, 1993. Units are µg m-3.

5. Perturbation Results for Southern California on September 25, 1996

Meteorological Patterns
Temperatures at inland locations in the South Coast Air Basin (SoCAB) were moderate on September 25, 1996, with peak daytime values reaching 25°C. Winds were light onshore during the day and stagnant during the evening. The total time required for air parcels to traverse the study region from west to east was calculated to be greater than 3 days.

Model Application
Routine hourly measurements made by the SCAQMD at their monitoring sites provided the meteorological inputs for the diagnostic meteorological model used to produce continuous fields for air quality calculations. These measurements include wind speed (29 sites), temperature (10 sites), relative humidity (10 sites), total solar radiation (4 sites) and ultraviolet solar radiation (1 site). Upper level wind speed, wind direction and temperature were measured at hourly intervals using a lower atmospheric radar profiler at the Los Angeles International Airport (LAX). In the current study, wind fields were specified with high numerical accuracy to improve self-consistency and reduce wind field divergence. Atmospheric mixing depths during the simulation were constructed using Holtzworth's method [42], the interpolated surface temperature throughout the modeling domain, and the vertical temperature profile measured at LAX.

The mobile source emissions inventory was calculated with the traffic emissions model EMFAC-7G featuring a day-specific temperature correction for evaporative emissions. Area source and small point source inventories within the modeling domain were based on the 1995 average-day emissions inventory provided by SCAQMD together with measured particle size and composition profiles [39, 40]. Similarly, large point source inventories were based on the 1997 average-day emissions inventory provided by SCAQMD together with measured particle size and composition profiles [39, 40]. To reflect changes in mobile sources, fertilizer and livestock emissions, the ammonia emissions inventory for the SoCAB [43] was updated to 1996 [3].

Results
Peak ozone concentrations measured at locations around central Los Angeles on September 25, 1996 were generally less than 100 ppb. Measurements of $PM_{2.5}$ concentrations at Riverside between the hours of 1400-1700 PST exceeded 75 $\mu g\ m^{-3}$, with higher concentrations predicted during the evening hours.

Figure 5-1 (a) shows the predicted regional pattern of 1hr-average ozone concentrations on September 25, 1996 at 1500 PST. The highest predicted ozone concentration is 120 ppb in the northeast corner of the domain that is downwind of the major emissions sources during this event. Concentrations around central Los Angeles are generally moderate, with predicted values of 70-80 ppb. Concentrations immediately dowwind of central Los Angeles are once again slightly lower than the regional average because they

are suppressed by emissions of fresh NO_X.

Figure 5-1(b) shows the predicted increase in regional ozone concentrations at 1500 PST on September 25, 1996 when temperature is uniformly perturbed by +2 K at all times and locations. Ozone concentrations in the eastern portion of the air basin increase by approximately 12 ppb in response to this change, with smaller increases of 1-3 ppb over the majority of the domain.

Figure 5-1(c) shows the predicted increase in regional ozone concentrations at 1500 PST on September 25, 1996 when temperature is uniformly perturbed by +5 K at all times and locations. The area of maximum ozone increase once again occurs in the regions with the highest base-case ozone concentrations. Peak ozone values increase by 33 ppb in response to the +5 K temperature perturbation, with smaller increases of 4-6 ppb predicted over much of the domain. A minor region with a 1 ppb ozone decrease in response to the +5 K temperature perturbation is observed near Fullerton.

Figure 5-2(a) shows the predicted regional pattern of 24-hr average $PM_{2.5}$ concentrations on September 25, 1996. The largest $PM_{2.5}$ concentrations 154 $\mu g\ m^{-3}$ are predicted to occur in the region west and northeast of Riverside where ammonia concentrations are very large leading to enhanced formation of particulate ammonium nitrate. The predicted concentration of $PM_{2.5}$ most other locations in the inland portion of the modeling domain is 40-80 $\mu g\ m^{-3}$. The moderate base-case temperatures during the current episode allow for the formation of significant quantities of particulate ammonium nitrate throughout the study region.

Figure 5-2(b) shows the predicted change in regional $PM_{2.5}$ concentrations on September 25, 1996 when temperature is uniformly perturbed by +2 K at all times and locations. $PM_{2.5}$ concentrations in the region north of Fontana and south of Riverside decrease by 11 $\mu g\ m^{-3}$ in response to this change. As discussed previously, the majority of this reduction is associated with the volatilzation of particulate ammonium nitrate as temperature increases. The locations west and northeast of Riverside with the highest base-case concentration of particulate nitrate (see Figure 5-2(a)) do not experience the largest reduction in $PM_{2.5}$ concentrations because of the high gas-phase ammonia concentrations in this region under the current meteorological conditions. Figure 5-2(b) also shows that regional average $PM_{2.5}$ concentrations are predicted to decrease by 2-5 $\mu g\ m^{-3}$ in response to the +2 K temperature perturbation. Scattered locations in the coastal evivornment experience miniscule increases of 0.2 $\mu g\ m^{-3}$ in $PM_{2.5}$ concentrations in response to a +2 K temperature perturbation.

Figure 5-2(c) shows the predicted change in regional $PM_{2.5}$ concentrations on September 25, 1993 when temperature is uniformly perturbed by +5 K at all times and locations. The trends shown in Figure 5-2(c) are very similar to those shown in Figure 5-2(b), but additional ammonium nitrate evaporates in the region northeast of Riverside around the high concentration plume formed by ammonia emissions from agricultural operations. The maximum decrease in $PM_{2.5}$ concentrations in this region is 29 $\mu g\ m^{-3}$.

Figure 5-3(b) shows the change in predicted regional ozone concentrations at 1500 PST on September 25, 1996 when temperature is uniformly perturbed by +2 K while relative humidity is held constant. This figure can be compared to Figure 5-1(b) which applied a +2 K temperature perturbation while absolute relative humidity was held constant. The spatial pattern of increased ozone between these two cases is very similar, but the magnitude of the ozone increase is larger for the case with higher relative humidity. The maximum increase in ozone concentrations shown in Figure 5-3(b) is 17 ppb compared to only 12 ppb in Figure 5-1(b). As discussed previously, water vapor is a source of hydroxyl radicals in urban areas, and so the increased humidity increases the reactivity of the atmosphere.

Figure 5-3(c) shows the change in predicted regional ozone concentrations at 1500 PST on September 25, 1993 when temperature is uniformly perturbed by +5 K while relative humidity is held constant. This figure can be compared to Figure 5-1(c) which applied a +5 K temperature perturbation while absolute relative humidity was held constant. Once again, the spatial pattern of the increased ozone concentration is similar, but the magnitude of the concentrations increase is enhanced by the addition of water vapor to the system. The maximum change in ozone concentration under this condition is 46 ppb (vs. 29 ppb for the case with lower humidity).

Figure 5-4(b) shows the change in predicted regional $PM_{2.5}$ concentrations on September 25, 1996 when temperature is uniformly perturbed by +2 K while relative humidity is held constant. This figure can be compared to Figure 5-2(b) which applied a +2 K temperature perturbation while absolute humidity was held constant. The region immediately west and northeast of Riverside experiences very little decrease in $PM_{2.5}$ concentrations when temperature is increased by +2 K with constant relative humdity because the high concencentration of gas-phase ammonia in the area and the constant water content of the aerosol maintain favorable conditions for nitrate formation even when temperature is increasing. The fringe around the high concentration region experiences a decrease in predicted $PM_{2.5}$ concentrations of 6 $\mu g\ m^{-3}$ under these conditions. Most inland portions of the domain experience a regional decrease in $PM_{2.5}$ concentrations of 1-3 $\mu g\ m^{-3}$.

Figure 5-4(c) shows the change in predicted regional $PM_{2.5}$ concentrations on September 25, 1996 when temperature is uniformly perturbed by +5 K while relative humidity is held constant. This figure can be compared to Figure 5-2(c) which applied a +5 K temperature perturbation while absolute humidity was held constant. The trends shown in Figure 5-4(c) match the results shown in Figure 5-4(b). The additional water in the case with constant relative humidity mitigates the reduction of ammonium nitrate associated with increased temperature. The largest reduction in $PM_{2.5}$ concentrations in response to the +5 K temperature perturbation with constant humidity is 15 $\mu g\ m^{-3}$ (vs. 29 $\mu g\ m^{-3}$ for the case with reduced humidity).

Figure 5-5(b) shows the change in predicted regional ozone concentrations at 1500 PST on September 25, 1996 in response to a uniform increase in mixing depths of +50%. The increased mixing depth has little impact on predicted ozone concentrations in this

pollution episode because base-case mixing depths are already relatively large. Predicted ozone concentrations in the eastern portion of the domain increase by a maximum of 11 ppb, with smaller increases of a few ppb (or even slight decreases) predicted for the central portion of the study region. The difference in the behavior of the pollution episode on September 25, 1996 vs September 9, 1993 emphasizes the need to model a large number of systems to explore the full range of possible outcomes.

Figure 5-5(c) shows the change in predicted regional ozone concentrations at 1500 PST on September 25, 1996 in repsonse to a uniform increase in wind speed of +20%. Predicted ozone concentrations in the wester portion of the model domain increase by 10 ppb in response to increased wind speeds, but the maximum predicted concentrations in the far northeast of the model domain decrease by 55 ppb. It is likely that the higher ozone concentrations were simply advected out of the study region by the increased winds. along the line connecting Claremont, Riverside, and Perris are decreased by 107 ppb.

Figure 5-6(b) shows the change in predicted regional $PM_{2.5}$ concentrations on September 25, 1996 in response to a uniform increase in mixing depth of +50%. A small increase in $PM_{2.5}$ concentrations of ~0.5 $\mu g\ m^{-3}$ is predicted to occur in the area downwind of Long Beach in response to this change, while concentrations in the eastern portion of the domain are predicted to decrease by ~6 $\mu g\ m^{-3}$. .

Figure 5-6(c) shows the change in predicted regional $PM_{2.5}$ concentrations on September 25, 1996 in response to a uniform increase in wind speed of +20%. The region with the highest base-case $PM_{2.5}$ concentrations is predicted to experience a decrease in $PM_{2.5}$ concentrations of 31 $\mu g\ m^{-3}$ in response to the increased wind speed, primarily through the enhanced dilution of primary ammonia emissions.

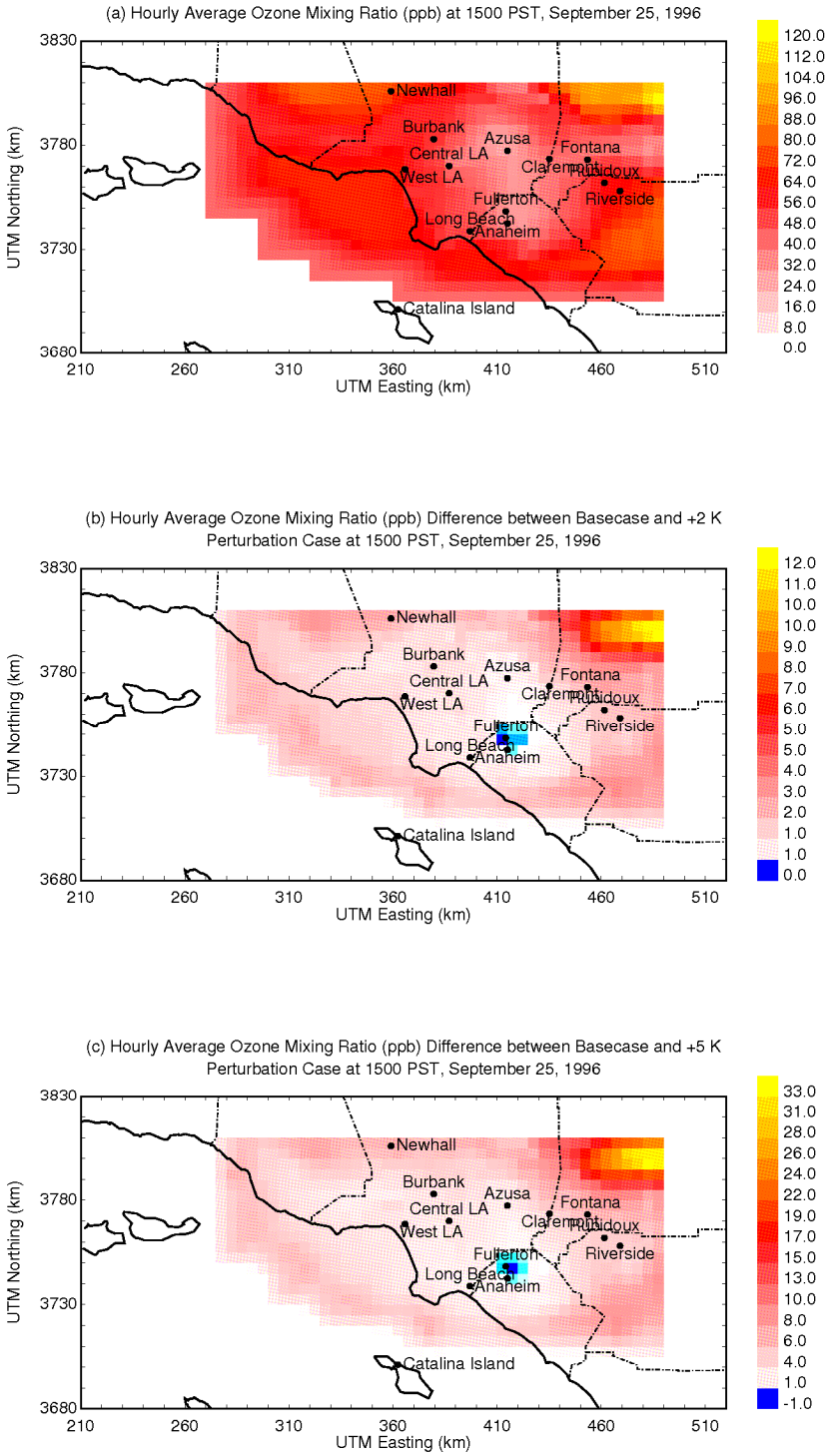

Figure 5-1: Hourly average ozone mixing ratio (panel a) and ozone mixing ratio difference in response to uniform temperature perturbations (panels b,c) at 1500 PST on September 25, 1996. Units are ppb.

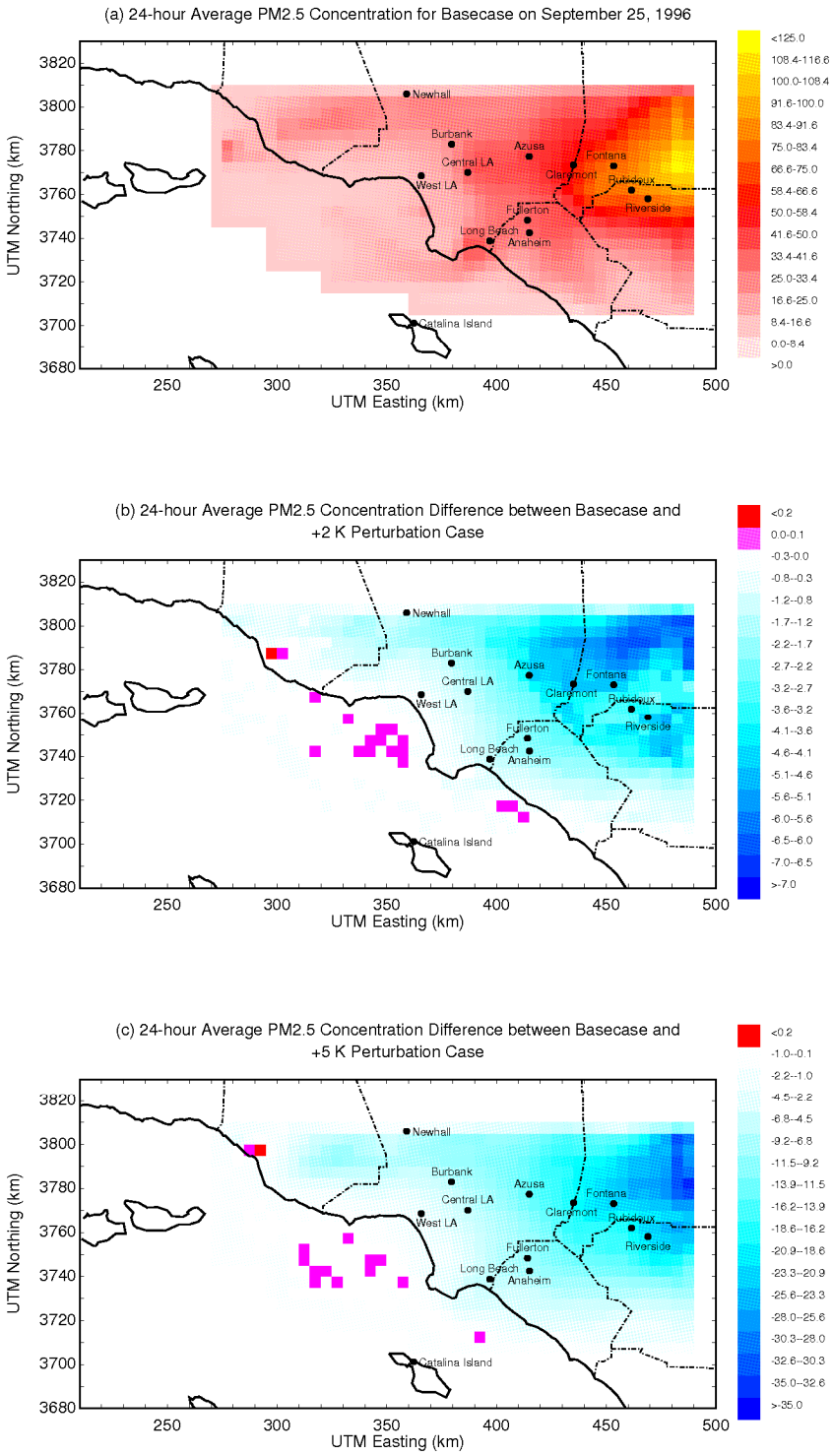

Figure 5-2: 24-hr average $PM_{2.5}$ concentration (panel a) and 24-hr average $PM_{2.5}$ concentration difference in response to uniform temperature perturbations (panels b,c) on September 25, 1996. Units are µg m-3.

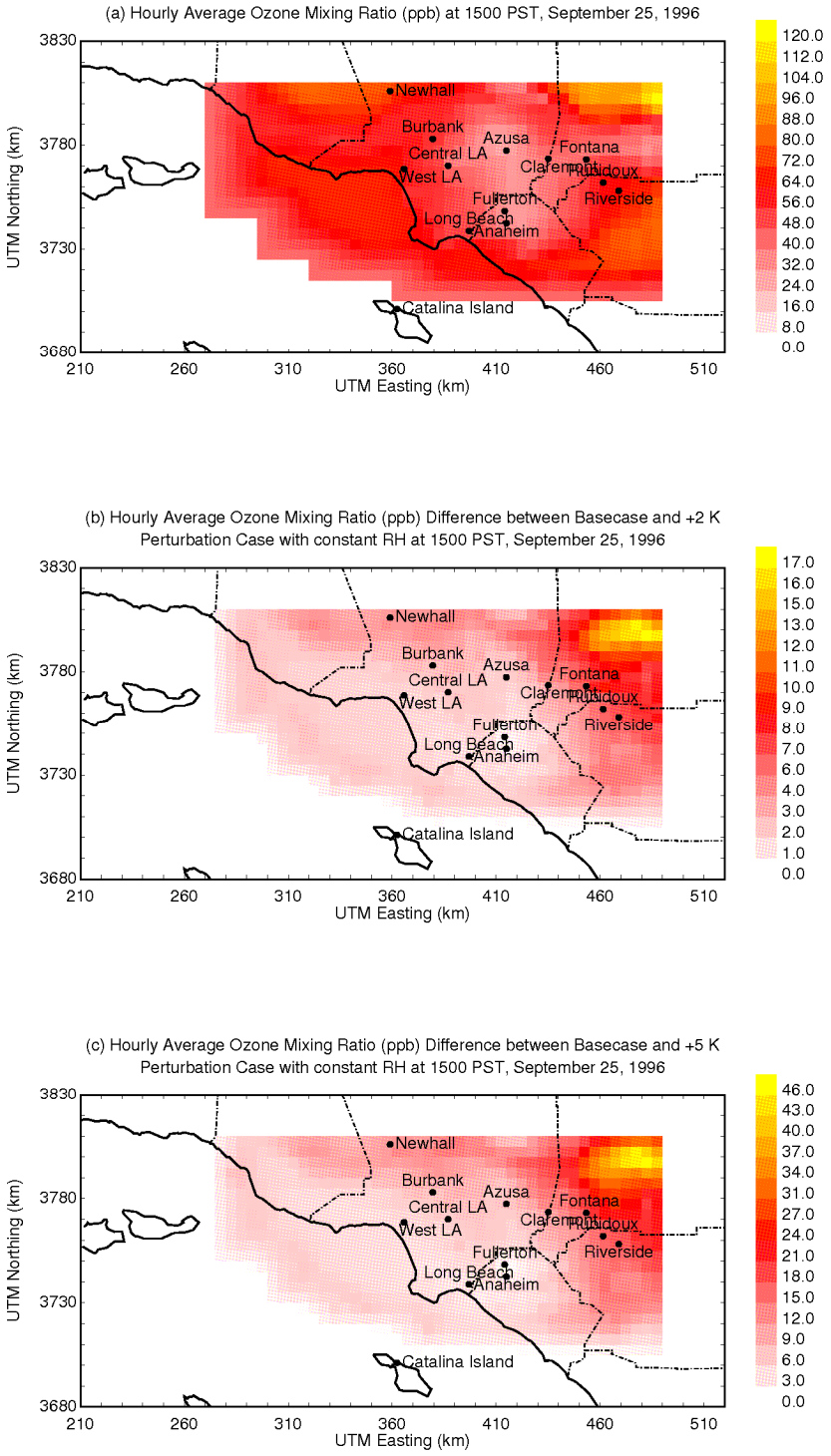

Figure 5-3: Hourly average ozone mixing ratio (panel a) and ozone mixing ratio difference in response to uniform temperature perturbations with constant relative humidity (panels b,c) at 1500 PST on September 25, 1996. Units are ppb.

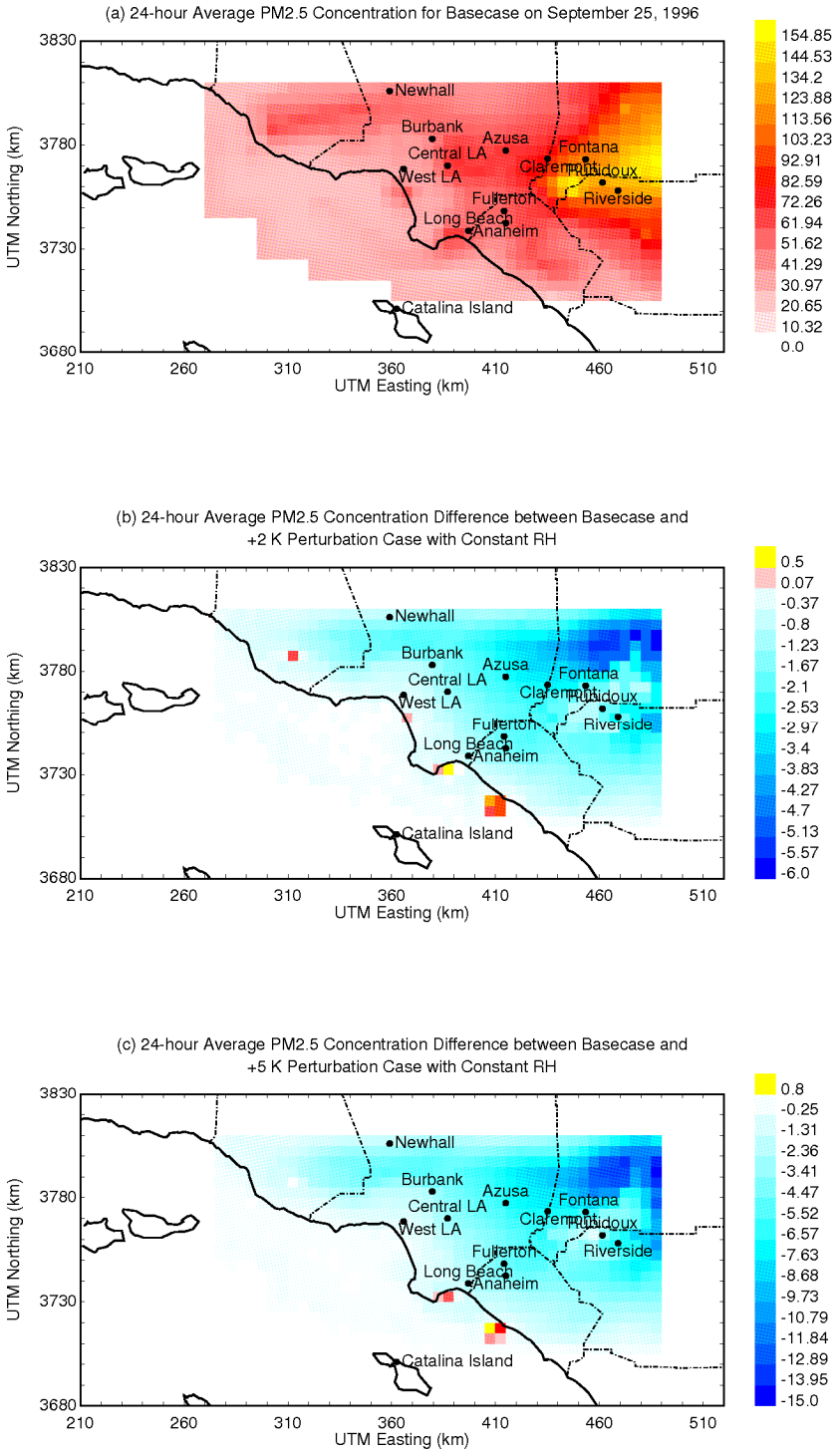

Figure 5-4: 24-hr average $PM_{2.5}$ concentration (panel a) and 24-hr average $PM_{2.5}$ concentration difference in response to uniform temperature perturbations with constant relative humidity (panels b,c) on September 25, 1996. Units are µg m-3.

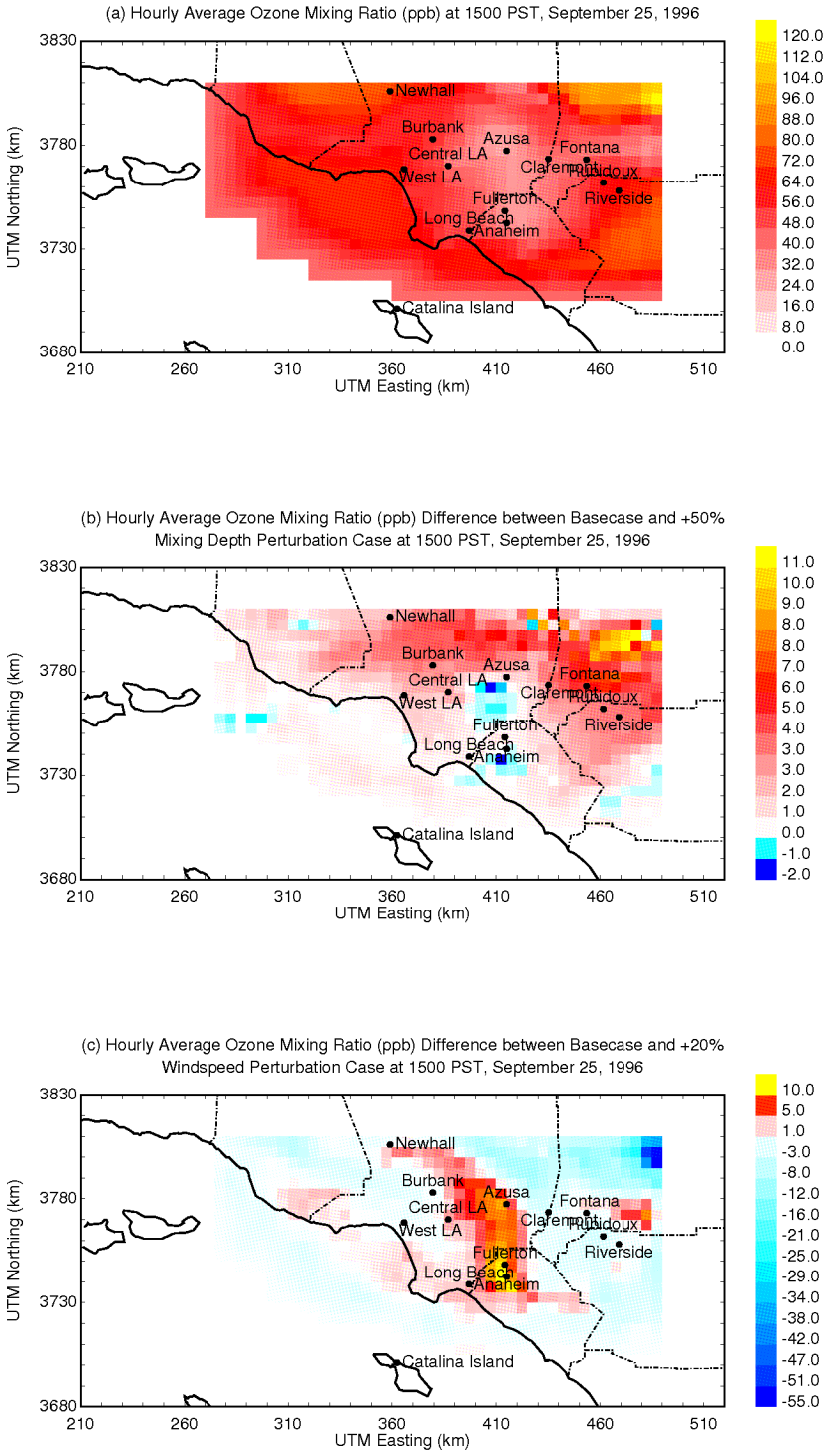

Figure 5-5: Hourly average ozone mixing ratio (panel a) and ozone mixing ratio difference in response to +50% increase in mixing depth (panels b) and +20% increase in wind speed (panel c) at 1500 PST on September 25, 1996. Units are ppb.

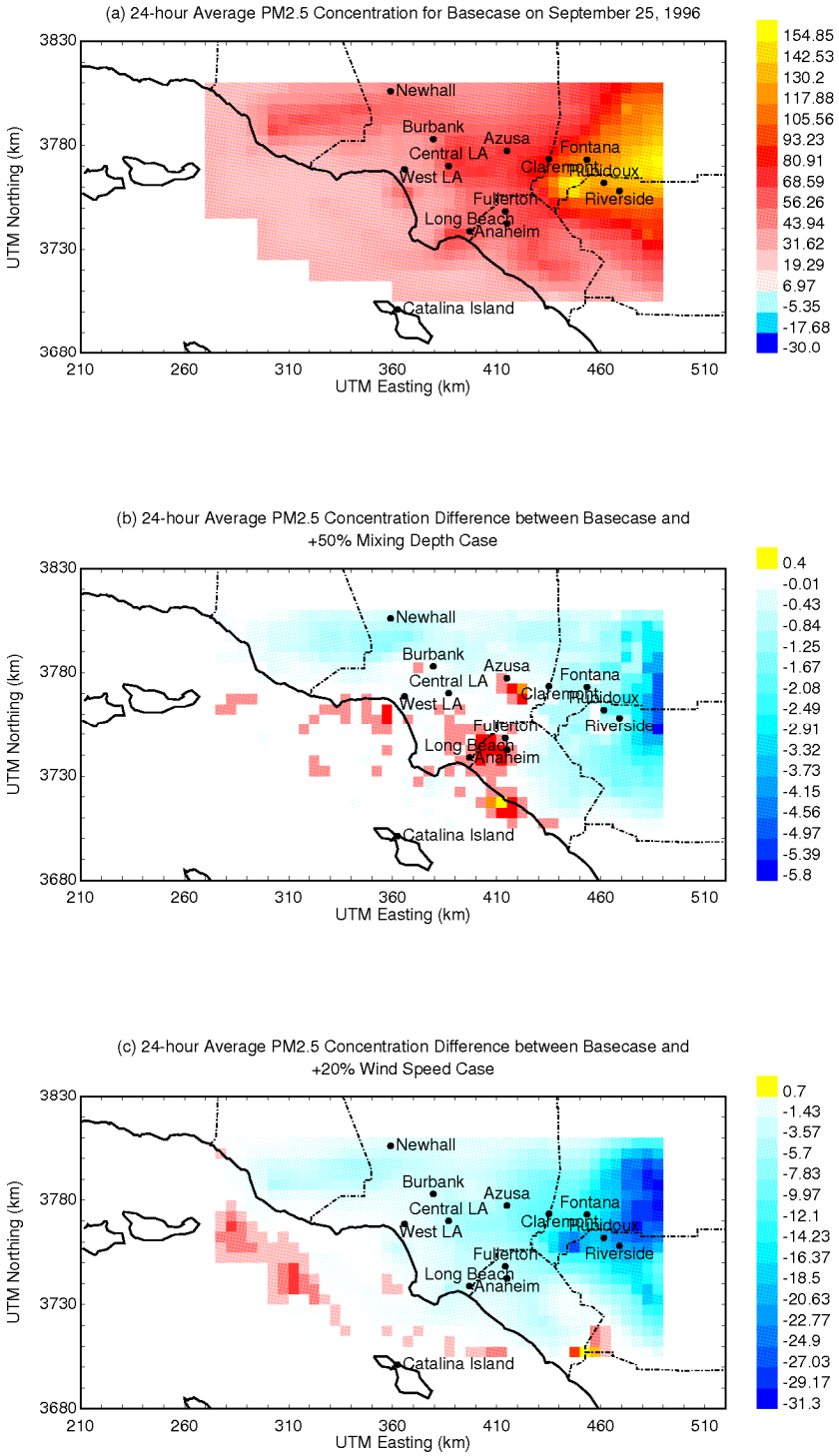

Figure 5-6: 24-hr average $PM_{2.5}$ concentration (panel a) and 24-hr average $PM_{2.5}$ concentration difference in response to +50% increase in mixing depth (panels b) and +20% increase in wind speed (panel c) on September 25, 1996. Units are µg m-3.

6. Perturbation Results for San Joaquin Valley on January 6, 1996

Meteorological Patterns

Even though the airborne particulate matter in the SJV and SoCAB has similar characteristics, each region has unique geography, emissions, and meteorological patterns. The SJV is approximately 400 km in length and 100 km in width. It is bounded on the west by the Coast Mountain range, on the east by the Sierra Nevada range and on the south by the Tehachapi Mountains. Elevated particulate matter concentrations in the SJV are usually associated with stagnant atmospheric conditions (low mixing depth and slow wind speed), which commonly occur between mid-November and mid-February. Typical meteorological patterns transport pollutants from north to south across the SJV. Temperatures during these episodes approach freezing during the night and reach a maximum value of ~15°C during the day.

Model Application [6]

Surface meteorological conditions within the study domain were measured by monitoring stations operated by CARB, the National Climatic Data Center (NCDC), and the California Irrigation Management System (CIMIS). Measured values of solar radiation (19 sites), relative humidity (70 sites), temperature (70 sites), wind speed (18 sites), wind direction (18 sites), and fog (10 airports) were used to specify surface meteorological conditions throughout the study region based on Goodin's interpolation procedure [30]. Reductions of the surface UV irradiants due to cloud cover were estimated using the empirical equation described by [44]. The surface fields were augmented with upper elevation measurements to create interpolated 3D fields for certain meteorological variables. Rawinsonde measurements collected near Fresno and Bakersfield provide vertical profiles of temperature and humidity in the domain. Rawinsonde and radar profiler measurements collected at six sites were used to interpolate the upper layer wind speed and wind direction. Transport was generally stagnant with low wind-flows from the northwest to the southeast during the study period. Based on the rawinsonde data, the Holtzworth method [42] was used to generate interpolated mixing depth fields that were verified and improved upon by detailed inspection of the temperature profiles. Calculated mixing depths were all well below 1000m during the 3 day simulation period, with a typical afternoon maximum mixing depth of approximately 700 m. Thus, the modeled column depth of 1100m encompasses the entire turbulent boundary layer during the modeling period.

The air pollutant emission rates in the SJV are the second largest in the state of California (preceded only by the SoCAB). Inventories describing the emissions of total organic gases (TOG), oxides of nitrogen (NO_X), oxides of sulfur (SO_X), ammonia (NH_3) and total suspended particulate matter (TSP) were compiled by CARB for the IMS95 study. All major area, point, and mobile source emissions within the study region were included in the inventory with a spatial resolution of 4 km and a temporal resolution of 1 h. Individual emissions records included a source classification category (SCC) number that could be used to assign detailed chemical speciation profiles to TOG and TSP emissions.

TOG and TSP profiles used in this study were based on previous emissions source tests [31-41, 45-47].

Models for the emission of airborne particulate matter from mobile sources are relatively new and often contain large sources of uncertainty. In the current study, the spatial and temporal distribution of TSP emissions for each mobile source category (diesel, non-catalystequipped gasoline, catalyst-equipped gasoline) was retained, but the emissions were scaled to match the product of vehicle miles traveled (VMT) and measured emissions factors [33, 36] appropriate for that category. This procedure increased the TSP emission rate from mobile sources (tailpipe+tire dust) in the study region from 5030 to 8460 kg day^{-1}.

Previous Analysis

The direct effect of temperature on ozone and particulate matter concentrations for the episode that occurred in the SoCAB on September 23-25, 1996 was examined previously by Aw and Kleeman [13]. The results of this analysis show that increased temperatures promote the formation of ozone and suppress the partitioning of semi-volatile species into the particle phase. Decreased relative humidity lowered both the ozone concentration and the concentration of semi-volatile particulate matter. Pollutant concentrations were not strongly sensitive to small variations in atmospheric mixing depths, likely because mixing depths were relatively large (100m – 1000m) during this study period. The results presented below repeat this analysis using the updated model described in Section 2.

Results

Measured ozone concentrations on January 6, 1996 were less than 40 ppb, reflecting the low photochemical activity during winter pollution events in the SJV. Particulate nitrate concentrations over the entire region built up to high levels during the stagnation event. Local emissions of carbonaceous aerosol also develop around urban areas where fuel combustion is used for home heating. Measured PM10 concentrations during the episode reached 150 $\mu g\ m^{-3}$ during the evening hours, with the majority of that material in the $PM_{2.5}$ size range.

Figure 6-1(a) shows the regional distribution of 1hr-average ozone concentrations in the SJV at 1500 PST on January 6, 1996. Peak ozone concentrations are 41 ppb across a wide portion of the study domain except in regions with large NO_X emissions where the ozone concentrations is titrate to very low values. The ozone suppression associated with the Highway 99 transportation corridor connecting Fresno, Visalia, and Bakersfield is clearly visible in this plot.

Figure 6-1(b) shows the regional distribution of 24-hr average $PM_{2.5}$ concentrations in the SJV on January 6, 1996. Peak $PM_{2.5}$ values reach 95 $\mu g\ m^{-3}$ around the urban locations of Fresno and Bakersfield due to the accumulation of wood smoke and other combustion particles combined with a regional background of ammonium nitrate particles.

Figure 6-1(c) shows the predicted increase in regional ozone concentrations at 1500 PST

on January 6, 1996 in the SJV when temperature is uniformly perturbed by +2 K at all times and locations. Ozone concentrations in the eastern portion of the air basin increase by only 4 ppb in response to this change, with smaller increases of ~2 ppb over the majority of the domain.

Figure 6-1(d) shows the predicted decrease in regional $PM_{2.5}$ concentrations on January 6, 1996 in the SJV when temperature is uniformly perturbed by +2 K at all times and locations. $PM_{2.5}$ concentrations in the band between Fresno and Visalia decrease by ~7 $\mu g\ m^{-3}$ in response to the increased temperature as ammonium nitrate partitions back to gas-phase ammonia and nitric acid.

Figure 6-1(e) shows the predicted increase in regional ozone concentrations at 1500 PST on January 6, 1996 in the SJV when temperature is uniformly increased by +5 K at all times and locations. Ozone concentrations in most locations increase by 7-8 ppb in response to this temperature increase except in the vicinity of Bakersfield where no change is observed. Fresh emissions of NO_X in the Bakersfield area titrate all ozone in this region to near zero. Previous studies have noted that the excess NO_X in the emissions inventory around Bakersfield appears to contradict measured concentrations in the region. Results in the area around Bakersfield are likely incorrect, but results for the remainder of the domain agree well with measurements and should be accurate.

Figure 6-1(f) shows the predicted decrease in regional $PM_{2.5}$ concentrations on January 6, 1996 in the SJV when temperature is uniformly perturbed by +5 K at all times and locations. $PM_{2.5}$ concentrations in the band between Fresno and Visalia decrease by ~15 $\mu g\ m^{-3}$ in response to the increased temperature as ammonium nitrate partitions back to gas-phase ammonia and nitric acid. The region immediately south of Visalia does not experience a large decrease in $PM_{2.5}$ concentrations because ammonia emissions in this region are very large, reducing the sensitivy of ammonium nitrate to temperature.

Figure 6-2(b) shows the change in predicted regional ozone concentrations at 1500 PST on January 6, 1996 when temperature is uniformly perturbed by +2 K while relative humidity is held constant. This figure can be compared to Figure 6-1(b) which applied a +2 K temperature perturbation while absolute humidity was held constant. The maximum increase in ozone concentrations in response to a +2 K temperature perturbaiton is +4 ppb in both cases, but the pattern of the increased concentrations changes slightly, with more production in the center of the SJV at higher humidity vs. around the edges of the SJV at lower relative humidity.

Figure 6-2(c) shows the change in predicted regional $PM_{2.5}$ concentrations on January 6, 1996 when temperature is uniformly perturbed by +2 K while relative humidity is held constant. This Figure can be compared to Figure 6-1(c) which applied a +2 K temperature perturbation while absolute humidity was held constant. The increased humidity offsets the tendancy of ammonium nitrate to partition to the gas phase. In the region immediately south of Visalia, a 3.7 $\mu g\ m^{-3}$ increase in $PM_{2.5}$ concentrations is predicted to occur when temperature increases by 2K. This region has large emissions of ammonia, which offsets the effect of increased temperature on ammonium nitrate

volatility. The base temperature is also low in the winter conditions during the current study, further reducing the sensitivity of ammonium nitrate to temperature increases. The increase of temperature in this region increases the formation rate of nitric acid faster than it increases the volatility of ammonium nitrate aerosol, leading to slightly higher predicted $PM_{2.5}$ concentrations. It should be noted that the location of the maximum increase is slightly south of the maximum base-case concentrations. The net effect of this temperature increase is to expand the region of maximum $PM_{2.5}$ concentrations during the current study. Other locations in the study region with lower amounts of excess gas-phase ammonia experience a decrease in $PM_{2.5}$ concentrations of 4.6 $\mu g\ m^{-3}$ in response to a +2 K temperature perturbation even when relative humidity remains constant.

Figure 6-2(d) shows the change in predicted regional ozone concentrations at 1500 PST on January 6, 1996 when temperature is uniformly perturbed by +5 K while relative humidity is held constant. This figure can be compared to Figure 6-1(d) which applied a +5 K temperature perturbation while absolute humidity was held constant. The maximum increase in ozone concentrations in response to this change in temperature is 11 ppb at higher relative humidity (vs. 8 ppb increase for the lower humdity case).

Figure 6-2(e) shows the change in predicted regional $PM_{2.5}$ concentrations on January 6, 1996 when temperature is uniformly perturbed by +5 K while relative humidity is held constant. This Figure can be compared to Figure 6-1(e) which applied a +5 K temperature perturbation while absolute humidity was held constant. The trends illustrate in Figure 6-2(e) match those noted previously for Figure 6-2(c), with a maximum increase in $PM_{2.5}$ concentrations of 8 $\mu g\ m^{-3}$ in the area south of Visalia, and a maximum decrease of 4.6 $\mu g\ m^{-3}$ around the edges of the model domain where gas-phase ammonia concentrations are predicted to be lower.

Figure 6-3(c) shows the change in predicted regional ozone concentrations at 1500 PST on January 6, 1996 in response to a uniform increase in mixing depths of +50%. Ozone concentrations increase at all locations in the modeling domain in response to this change except for a few boundary cells at the extreme southern end. The maximum increase is 9 ppb along the transportation corridor connecting Fresno and Visalia, and in other regions of the domain where fresh NO_X emissions titrated ozone concentrations. The increased mixing depth reduces NO_X concentrations close to the ground, leading to higher surface ozone concentrations.

Figure 6-3(d) shows the change in predicted regional $PM_{2.5}$ concentrations on January 6, 1996 in response to a uniform increase in mixing depths of +50%. Predicted $PM_{2.5}$ concentrations immediately north of Bakersfield increase by +4.6 $\mu g\ m^{-3}$ in response to the increased mixing depth because the dilluted NO_X concentrations form more nitric acid which interacts with the ammonia plume just north of that location. As noted previously, the high NO_X emissions in the Bakersfield region are an artifact of the emissions inventory used in the current study, and so this increase in concentrations is likely also an artifact. $PM_{2.5}$ concentrations at locations farther north in the domain are predicted to undergo slight decreases or increases associated with the enhanced mixing of pollutants aloft to the surface.

The results of ozone and $PM_{2.5}$ predictions associated with an increase in wind speed are not available at the present time. These data will be added at a later date.

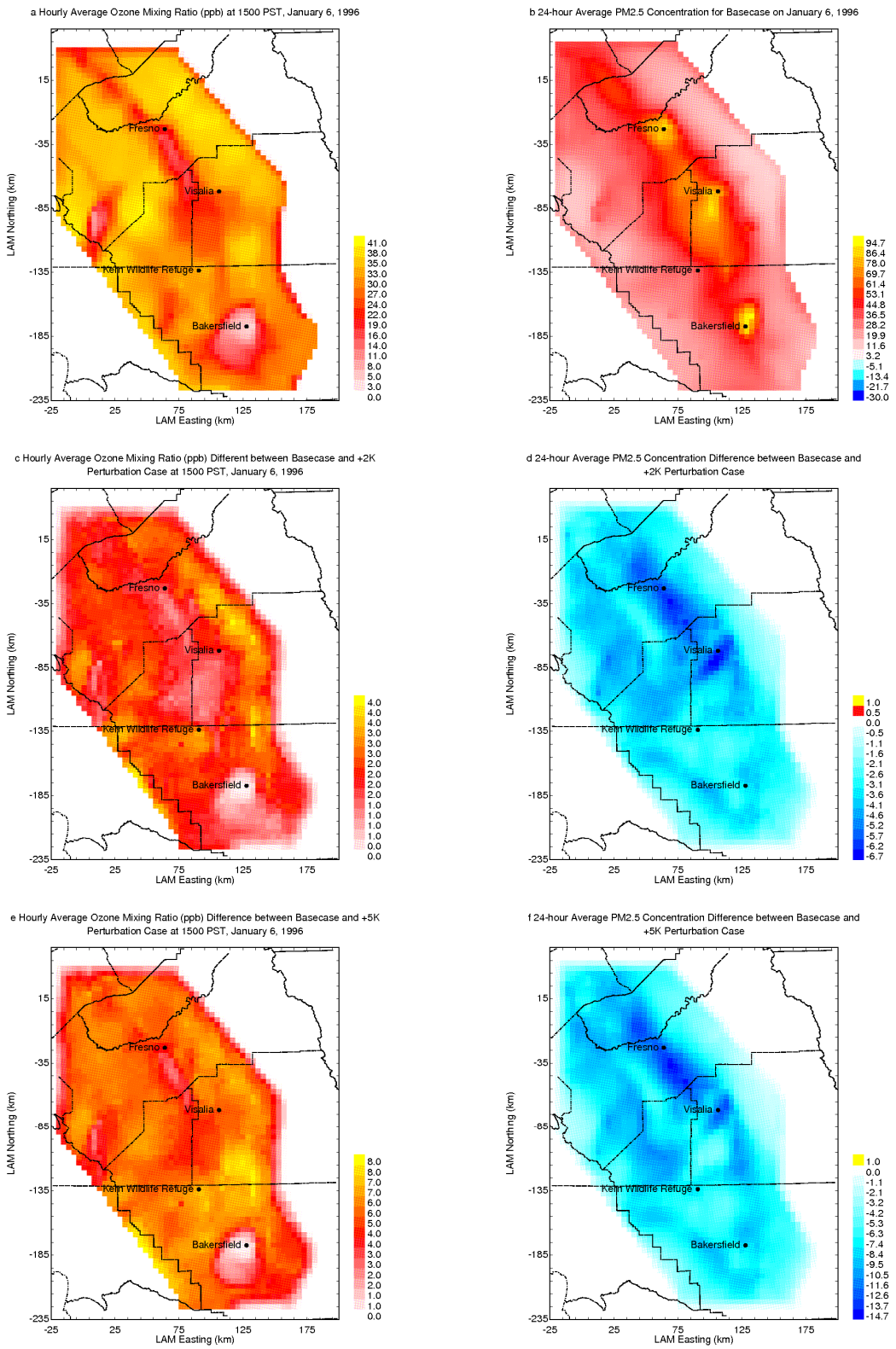

Figure 6-1: Pollutant concentrations in the San Joaquin Valley on January 6, 1996. (a) Hourly-average ozone mixing ratio (ppb) and (b) 24-hr average $PM_{2.5}$ concentration (μg m^{-3}). Panels (c-f) show the change in pollutant concentrations caused by a +2 K and +5 K temperature perturbation.

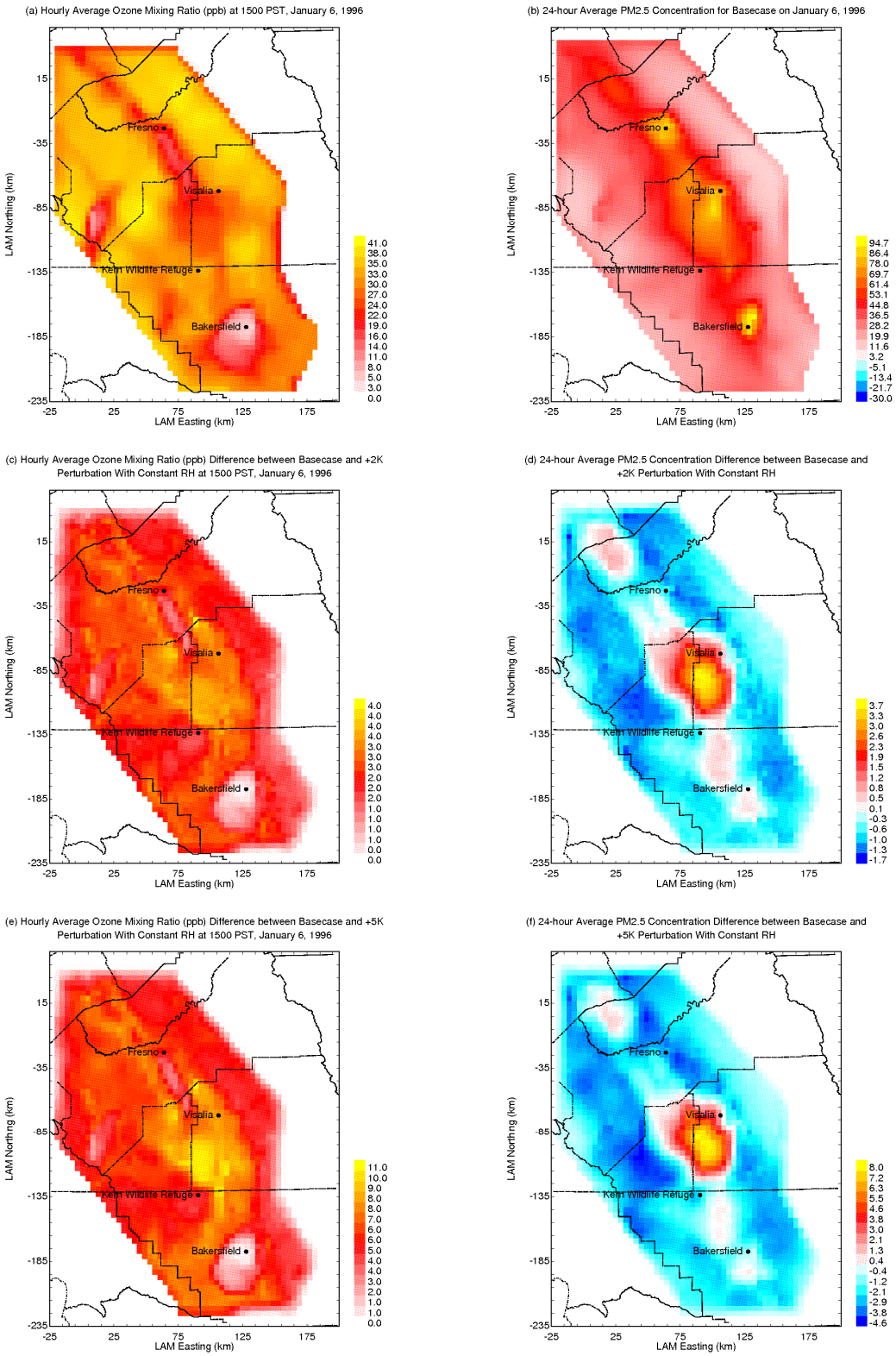

Figure 6-2: Pollutant concentrations in the San Joaquin Valley on January 6, 1996. (a) Hourly-average ozone mixing ratio (ppb) and (b) 24-hr average $PM_{2.5}$ concentration (µg m^{-3}). Panels (c-f) show the change in pollutant concentrations caused by a +2 K and +5 K temperature perturbation with constant relative humidity.

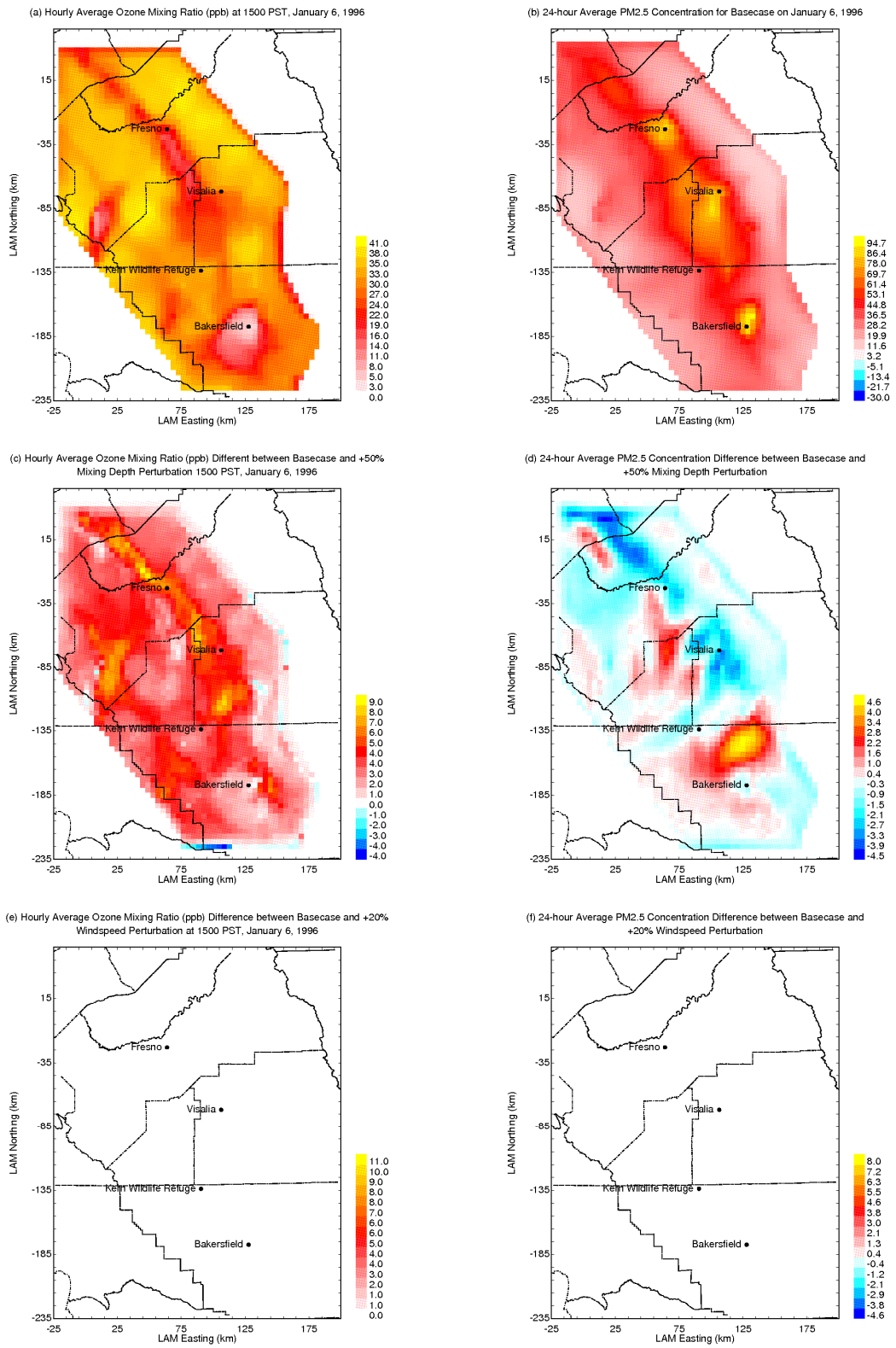

Figure 6-3: Pollutant concentrations in the San Joaquin Valley on January 6, 1996. (a) Hourly-average ozone mixing ratio (ppb) and (b) 24-hr average $PM_{2.5}$ concentration (µg m^{-3}). Panels (c-d) show the change in pollutant concentrations caused by a +50% increase in mixing depth.

7. Frequency of Future Stagnation Events

A large body of previous work, and the sensitivity studies above, indicate that frequency of atmospheric stagnation events and possibly the occurrence of warm synoptic events plays a significant role in determining the number of days with unhealthy air quality each year in California. Each of the pollution episodes studied in the preceding Sections 3-5 was driven by an atmospheric stagnation event. High pressure systems situated just off the coast of California produced warm temperatures aloft that encouraged elevated temperature inversions and weak winds. Climate change will affect the frequency and severity of atmospheric stagnation events in California. A method is needed to asses how this will influence air quality problems.

One method to quantitatively investigate the effect climate on the frequency of atmospheric stagnation events in California is to develop a simple linear statistical downscaling technique that relates large-scale meteorological information to air quality in the SJV and SoCAB. As part of the current project, linear regressions were calculated between meteorological information from the NCEP/NCAR Reanalysis Model output and ozone concentrations at Visalia (SJV) and Riverside (SoCAB) over the historical period 1980-2005. The NCEP/NCAR output has the same approximate spatial scale as GCM predictions (~200km horizontal). Linear regressions relating pollutant concentrations and large-scale atmospheric measures in the NCEP/NCAR output provide a statistical method to investigate the tendancy of future meteorology to encourage or discourage future air pollution events.

Correlations were investigated between daily maximum 1-hr average ozone concentrations and the following meteorological variables: temperature at 850 millibars (T850), temperature at 925 millibars (T925), temperature at 1000 millibars (T1000), wind speed at 850 millibars (wsp850), wind speed at 925 millibars (wsp925), and wind speed at 1000 millibars (wsp1000). Lagged versions of each variable were also considered in the multivariate statistical analysis. The most significant variable associated with daily maximum 1-hr average ozone concentrations measured at locations in both the SJV and the SoCAB was found to be temperature at 850 millibars (T850) on the same day.

The slope of the linear regression relating ozone and T850 changes as a function of the time period that was considered. Years prior to 1992 have a somewhat steeper regressions coefficient (slope) between ozone and T850 than years after 1996 for locations in both the SJV and SoCAB. This change in behavior likely results from the introduction of reformulated gasoline in California in the early-mid 1990's. The slope of the linear correlation curve relating ozone and T850 also changes as a function of month. August has the steepest linear relationship between ozone and T850, that is, ozone concentration changes in August are most responsive to changes in lower tropospheric temperature. Lesser slopes are observed for May – July, and September. This behavior is likely related to changes in biogenic emissions, absolute temperature, and possibly the length of day, but these hypotheses warrant future investigation to determine what mechanisms lie behind these statistical linkages.

Global Climate Models are best suited to characterize large scale patterns and, hopefully, long-term trends, and less so for shorter term variability on fine (hourly) time scales. The statistical correlations identified in the daily maxium 1-hr average ozone concentrations should not be used with GCM output to predict future daily maximum 1-hr average ozone concentrations, but the GCM output does not generally provide information at time intervals shorter than one day and their spatial resolution is coarse, of order 200-250km, so it may be more appropriate if longer averaging times are used. One method that appears to yield useful insight is to apply longer averaging times is to consider the relationship between monthly average T850 in the SJV and SoCAB vs. the number of days per month that exceeded the threshold of 90 ppb.

It is important to determine if the time averaging methodology can be shown to operate in the historical record. Figure 7-1 shows the number of days each month with 1-hr average ozone greater than 90 ppb vs. monthly average T850 at Riverside (SoCAB) and Visalia (SJV) for May – October during the years 1996-2003. Both locations exhibit a correlation slope between 0.7 – 0.75 and a correlation coefficient (R^2) of approximately 0.55. The correlations illustrated in Figure 7-1 can also be observed in the data prior to 1992, but the regression coefficients (slopes) are different as discussed above. The relationships illustrated in Figure 7-1 will be used to predict the degree to which future climate will encourage the formation of higher ozone concentrations.

Figure 7-2 shows the predicted number of days each year that would have 1-hr average ozone concentrations greater than 90 ppb at Riverside if the emissions and upwind boundary conditions for the SoCAB remained unchanged between the years 2000 – 2100. The exceedence days shown in Figure 7-2 are not intended to predict actual conditions in the future, since the climate model temperature are only a small subset of possible future climate in the California regiona, and future emissions and upwind boundary conditions will change in response to population growth, control programs, and new technology. Rather, the trends illustrated in Figure 7-2 illustrate the degree to which future meteorology will encourage a greater frequency of high ozone events relative to present day conditions. Figure 7-2 was construced using GCM predictions from the GFDL model for monthly average T850 over the indicated time period, combined with the correlations illustrated in Figure 7-1. The GFDL simulations were performed using both the SREAS A2 and B1 scenarios, representing medium-high and low, respectively, greenhouse gas (GHG) emissions scenario, prescribed by the IPCC; see http://www.grida.no/climate/ipcc_tar/wg1/474.htm. All of the trends illustrated in Figure 7-2 are positive, indicating that climate warming will tend to produce an increased frequency of high ozone days in the SoCAB in the future. The A2 emissions scenario (higher GHG emissions case) has a greater upward trend after the year 2050 than the B1 emissions scenario (lower GHG emissions case).

Figure 7-3 shows the predicted number of days each year that would have 1-hr average ozone concentrations greater than 90 ppb at Visalia if the emissions and upwind boundary conditions for the SJV remained unchanged between the years 2000 – 2100. Once again, this figure is designed to show the tendancy for future meteorology to

encourage ozone formation relative to present conditions (not predict future ozone concentrations). The GFDL simulations combined with the statistical downscaling technique once again predict a greater tendancy for future meteorology to encourage an increased frequency of high ozone days, with more exceedences associated with the A2 emissions scenario.

The results shown in Figures 7-2 and 7-3 were constructed using predictions from the GFDL Global Climate Model. A variety of other climate models could also be used for this analysis, but most current models predict some warming of the toposphere in the coming century. It is important to know that the GFDL model is among the class of models that is more resonsive to changes in GHG forceing—it produces a higher degree of warming, though not the highest, than other models to a prescribed change in atmospheric CO2 concentrations. Thus, the broad trends illustrated in Figure 7-2 and 7-3 are likely similar to those that would be predicted by any GCM, although the rate of change associated with each model and each GHG emissions scenario may differ slightly.

Downscaling techniques such as those illustrated in figure 7-1 to 7-3 were also investigated for airborne particulate matter, but no robust association could be found. Work is continuing to develop a statistical downscaling technique for $PM_{2.5}$. One possible outcome of this analysis is that increased temperatures could lower $PM_{2.5}$ concentrations during the early fall period that has historically experienced the highest $PM_{2.5}$ concentrations in the SoCAB, but $PM_{2.5}$ concentrations later in the year could increase as temperatures rise during the winter months. However, the sense of these changes are still not very clear, because it is necessary to determine whether vertical temperature gradients, including inversions will increase or decrease and how wind speeds and directions will be affected as California's regional climate changes. Dynamically downscaled regional atmospheric simulations may be necessary to augment and clarify the larger scale indications from the GCMs. Thus, climate change may not lower the peak $PM_{2.5}$ concentration experienced during the year, and climate change may alter the length of the $PM_{2.5}$ season in unforseen ways. These questions will be investigated in the second phase of the project.

One obvious correlation between future meteorology and $PM_{2.5}$ concentrations that can be investigated at the current time is the effect of rainfall. Rain events remove particles from the atmosphere with great efficiency. More frequent precipitation events will reduce airborne particulate matter concentrations, while less frequent precipitation events will allow for the possibility that airborne particulate matter concentrations will increase.

Figure 7-4 shows the number of predicted fall days each year with precipitation greater than 0.02mm in the SoCAB over the time period 2000 – 2100. Fall days (in the months of September – November) were chosen because these months historically have the highest $PM_{2.5}$ concentrations in the SoCAB. Predictions of precipitation were taken from GFDL simulations. No clear trends are apparent in the precipitation frequency for either the A2 or B1 GHG emissions scenario.

Figure 7-5 shows the number of predicted winter days each year with precipitation

greater than 0.02mm in the SJV over the time period 2000 – 2100. Winter days (in the months of December – February) were chose because these months historically have the highest $PM_{2.5}$ concentrations in the SJV. Again, no clear trend is obvious in Figure 7-5.

The lack of a clear precipitation trend is consistent with the observation that GCM's do not predict consistent trends for the frequency of future precipitation. There is likely a large amount of uncertainty associated with the results shown in Figures 7-4 and 7-5. As a result, no conclusions about the effect of precipitation on $PM_{2.5}$ concentrations can be made at this time.

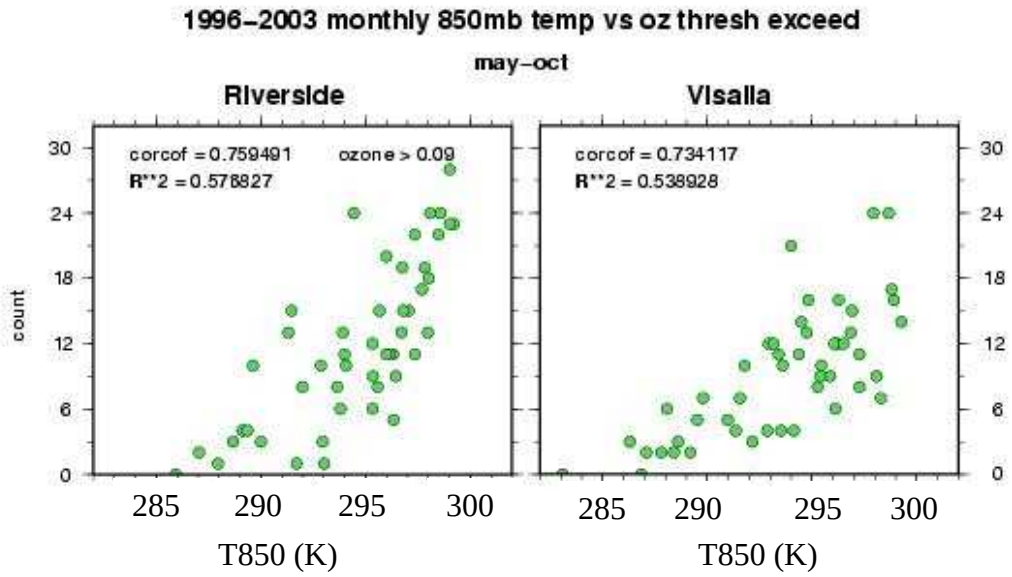

Figure 7-1: Number of days each month with 1-hr average ozone greater than 90ppb vs. monthly average T850 at Riverside (SoCAB) and Visalia (SJV) for May – October during the years 1996-2003.

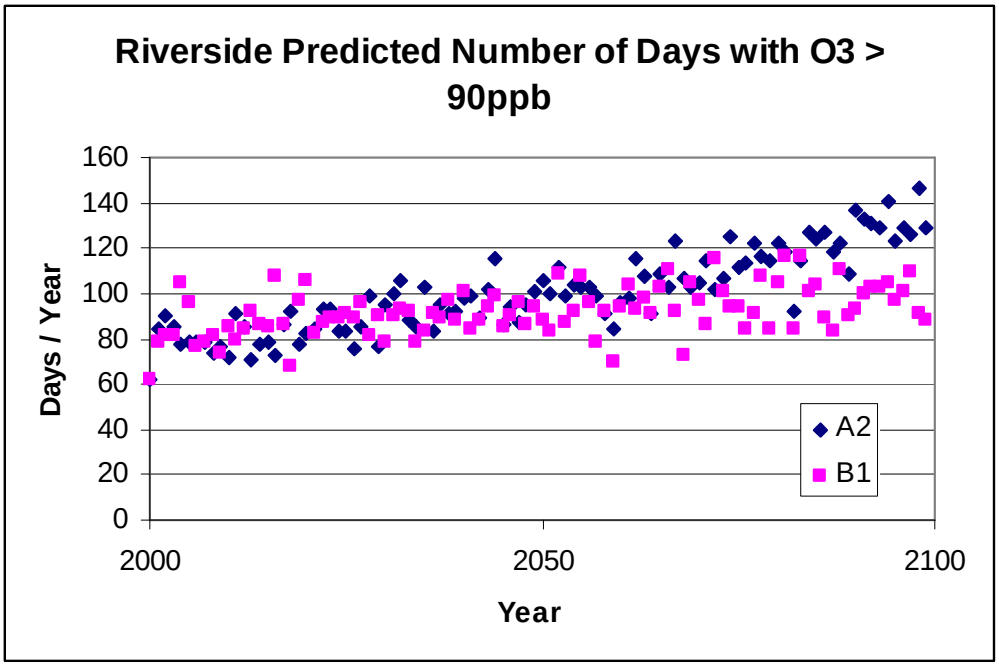

Figure 7-2: GFDL predictions for monthly mean 850 millibar temperatures in the SoCAB converted to estimates of the number of days each year with ozone greater than 90 ppb at Riverside. The results assume that emissions in the SoCAB remain constant while global emissions follow IPCC projections. Global emissions scenario A2 has higher global CO2 emissions than scenario B1.

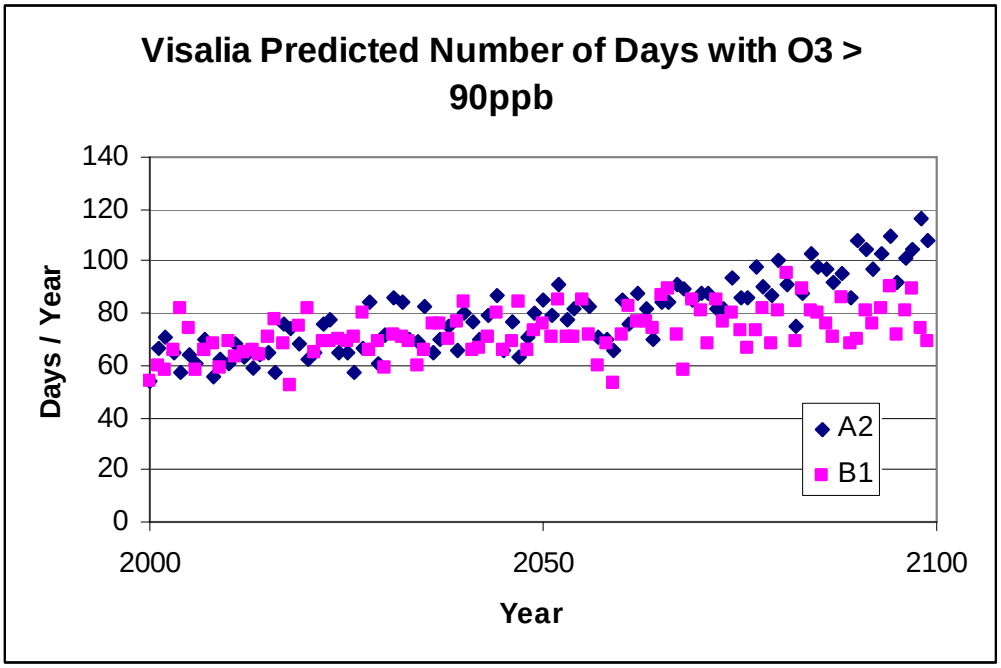

Figure 7-3: GFDL predictions for monthly mean 850 millibar temperatures in the SJV converted to estimates of the number of days each year with ozone greater than 90 ppb at Visalia. The results assume that emissions in the SJV remain constant while global emissions follow IPCC projections. Global emissions scenario A2 has higher global CO2 emissions than scenario B1.

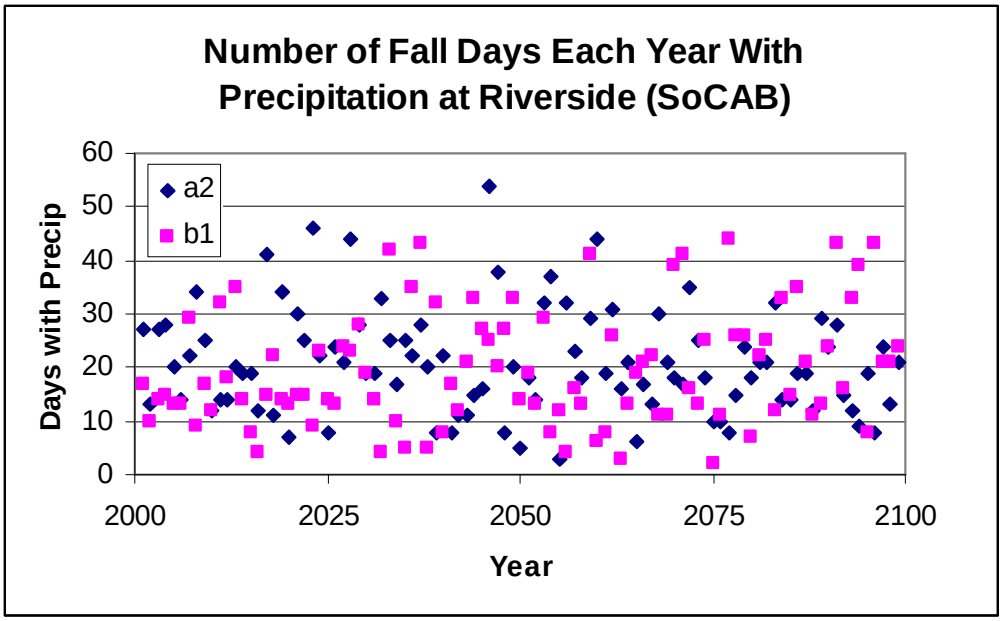

Figure 7-4: GFDL predictions for the number of fall days each year with precipitation > 0.02mm in the SoCAB at Riverside. Fall corresponds to the historical period with the highest $PM_{2.5}$ concentrations in the SoCAB. Increased precipitation greatly reduces airborne particulate matter concentrations.

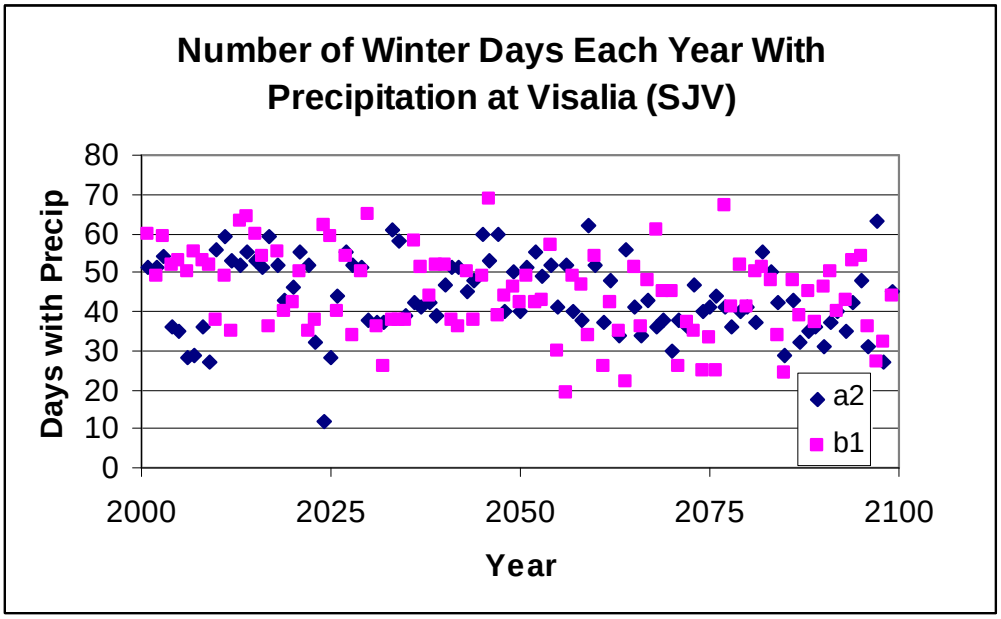

Figure 7-5: GFDL predictions for the number of winter days each year with precipitation > 0.02mm in the SJV at Visalia. Winter corresponds to the historical period with the highest $PM_{2.5}$ concentrations in the SJV. Increased precipitation greatly reduces airborne particulate matter concentrations.

8. Conclusions

Figure 8-1 summarizes the range of changes in predicted ozone and $PM_{2.5}$ concentrations resulting from all the perturbations studied in the current project. The bars shown in Figure 8-1 illustrate the largest change in pollutant concentrations predicted anywhere in the domain, while the circles illustrate the change in the maximum concentrations. When the circles are located close to the extreme values of the bars, it shows that the greatest change in concentration occurs at the location of maximum concentration.

Figure 8-1 illustrates that increasing wind speed results in the greatest decrease in ozone and $PM_{2.5}$ concentrations in the SoCAB during both the September 7-9, 1993 episode and the September 23-25, 1996 episode. These reductions occur at the location of maximum base-case concentrations except for the case of ozone in the SoCAB on September 25, 1996 when maximum ozone concentrations are not significantly affected by wind speed.

Figure 8-1 also shows that increasing temperature at constant absolute humidity generally increases peak ozone concentrations and decreases peak $PM_{2.5}$ concentrations in all the episodes studied. Part of this temperature effect on $PM_{2.5}$ concentrations may be caused by reduced particle water content, since relative humidity decreases as temperature increases and absolute humidity remains constant.

Increasing temperature at constant relative humidity increases predicted ozone concentrations even further due to the enhanced production of hydroxyl radical. The increased absolute humidity also mitigates the reduction in $PM_{2.5}$ concentrations, and even increases $PM_{2.5}$ concentrations in the SJV in regions with large excesses of gas-phase ammonia.

Figure 8-1 generally shows that increasing mixing depths usually increases surface ozone concentrations because the extra volume allows for increased dilution of fresh NO_X emissions, reducing the titration of surface ozone concentrations. This effect may not be significant at the location of maximum ozone concentration. The increased mixing depth usually also reduces primary $PM_{2.5}$ concentrations through increased dillution. This trend generally holds true in the SoCAB, but isolated regions in the SJV may experience slight increases in $PM_{2.5}$ concentrations in response to increased mixing depth.

The trends illustrated in Figure 8-1 provide a mechanistic understanding of the likely impacts of climate change on air quality in California and suggest some preliminary conclusions. Temperatures will almost certainly rise in future air pollution episodes, leading to increased ozone concentrations. Particulate nitrate concentrations are likely to decrease slightly in the SoCAB as temperatures rise, but they may stay constant or even increase slightly in the SJV depending on the corresponding change to humidity. A regional meteorological model will be used to dynamically downscale representative stagnation episodes in the future during the second phase of this project to support a more detailed analysis of how future meteorology will change pollutant concentrations.

GCM predictions from the GFDL model suggest that climate change will increase the frequency of warm synoptic events that encourage ozone formaton in both the SJV and the SoCAB. Global emissions scenarios that have higher carbon emissions appear to encourage this trend. Future emissions reduction and the adoption of new technology will need to offset this tendancy for the formation of ozone pollution episodes in order to protect the public health of California residents.

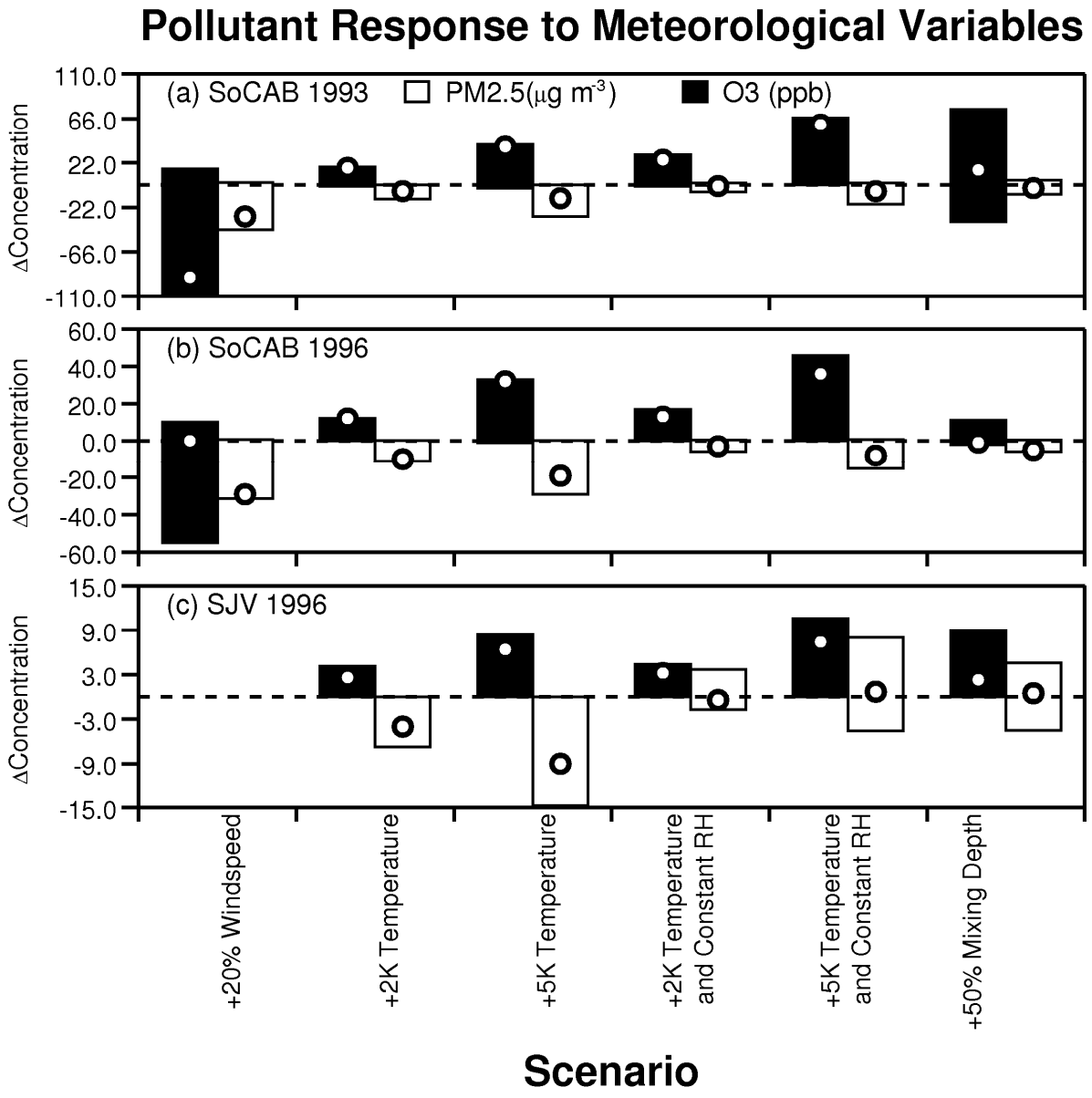

Figure 8-1: Summary of pollutant response to meteorological perturbations during pollution episodes that occurred in (a) Southern California September 9, 1993, (b) Southern California September 25, 1996, and (c) the San Joaquin Valley January 6, 1996. The bars represent the range of concentration change at any location in the modeling domain in response to the indicated perturbation. The circles represent the concentration change at the location of the maximum concentration for each pollutant.

9. References

1. Fraser, M.P., M.J. Kleeman, J.J. Schauer, and G.R. Cass, *Modeling the atmospheric concentrations of individual gas-phase and particle-phase organic compounds.* Environmental Science & Technology, 2000. **V34 N7**(APR 1): p. 1302-1312.
2. Griffin, R.J., D. Dabdub, M.J. Kleeman, M.P. Fraser, G.R. Cass, and J.H. Seinfeld, *Secondary organic aerosol - 3. Urban/regional scale model of size- and composition-resolved aerosols.* Journal of Geophysical Research-Atmospheres, 2002. **107**(D17): p. art. no.-4334.
3. Kleeman, M.J., L.S. Hughes, J.O. Allen, and G.R. Cass, *Source contributions to the size and composition distribution of atmospheric particles: Southern California in September 1996.* Environmental Science & Technology, 1999. **33**(23): p. 4331-4341.
4. Kleeman, M.J. and G.R. Cass, *A 3D Eulerian source-oriented model for an externally mixed aerosol.* Environmental Science & Technology, 2001. **35**(24): p. 4834-4848.
5. Mysliwiec, M.J. and M.J. Kleeman, *Source apportionment of secondary airborne particulate matter in a polluted atmospbere.* Environmental Science & Technology, 2002. **36**(24): p. 5376-5384.
6. Held, T., Q. Ying, A. Kaduwela, and M. Kleeman, *Modeling particulate matter in the San Joaquin Valley with a source-oriented externally mixed three-dimensional photochemical grid model.* Atmospheric Environment Part a-General Topics, 2004. **38**(22): p. 3689-3711.
7. Hayhoe, K., D. Cayan, C.B. Field, P.C. Frumhoff, E.P. Maurer, N.L. Miller, S.C. Moser, S.H. Schneider, K.N. Cahill, E.E. Cleland, L. Dale, R. Drapek, R.M. Hanemann, L.S. Kalkstein, J. Lenihan, C.K. Lunch, R.P. Neilson, S.C. Sheridan, and J.H. Verville, *Emissions pathways, climate change, and impacts on California.* PROCEEDINGS OF THE NATIONAL ACADEMY OF SCIENCES OF THE UNITED STATES OF AMERICA, 2004. **101**(34): p. 12422-12427.
8. Kim, J., *A projection of the effects of the climate change induced by increased CO2 on extreme hydrologic events in the western U.S.* Climate Change, 2005. **68**: p. 153-168.
9. Kim, J., *A nested modeling study of elevation-dependent climate change signals in California induced by increased atmospheric CO2.* Geophysical Research Letters, 2001. **28**: p. 2951-2954.
10. Mickley, L.J., D.J. Jacob, B.D. Field, and D. Rind, *Effects of future climate change on regional air pollution episodes in the United States.* Geophysical Research Letters, 2004. **31**(24).
11. Hogrefe, C., B. Lynn, K. Civerolo, J.Y. Ku, J. Rosenthal, C. Rosenzweig, R. Goldberg, S. Gaffin, K. Knowlton, and P.L. Kinney, *Simulating changes in regional air pollution over the eastern United States due to changes in global and regional climate and emissions.* Journal of Geophysical Research, 2004. **109**(D22).
12. Langner, J. and R. Bergstrom, *Impact of climate change on surface ozone and deposition of sulphur and nitrogen in Europe.* Atmospheric Environment, 2005.

39: p. 1129-1141.
13. Aw, J. and M.J. Kleeman, *Evaluating the first-order effect of intraannual temperature variability on urban air pollution.* Journal of Geophysical Research-Atmospheres, 2003. **108**(D12).
14. Ying, Q. and M.J. Kleeman, *Source contributions to the regional distribution of secondary particulate matter in California.* Atmospheric Environment, 2005. **Accepted for publication**.
15. Carter, W.P.L., *A Detailed Mechanism for the Gas-Phase Atmospheric Reactions of Organic-Compounds.* Atmospheric Environment Part a-General Topics, 1990. **24**(3): p. 481-518.
16. Pandis, S.N., R.A. Harley, G.R. Cass, and J.H. Seinfeld, *Secondary Organic Aerosol Formation and Transport.* Atmospheric Environment Part a-General Topics, 1992. **26**(13): p. 2269-2282.
17. Odum, J.R., T. Hoffmann, F. Bowman, D. Collins, R.C. Flagan, and J.H. Seinfeld, *Gas/particle partitioning and secondary organic aerosol yields.* Environmental Science & Technology, 1996. **30**(8): p. 2580-2585.
18. Griffin, R.J., D. Dabdub, and J.H. Seinfeld, *Secondary organic aerosol - 1. Atmospheric chemical mechanism for production of molecular constituents.* Journal of Geophysical Research-Atmospheres, 2002. **107**(D17).
19. Griffin, R.J., D. Dabdub, and J.H. Seinfeld, *Development and initial evaluation of a dynamic species-resolved model for gas phase chemistry and size-resolved gas/particle partitioning associated with secondary organic aerosol formation.* Journal of Geophysical Research, 2005. **110**(D5).
20. Pun, B.K., R.J. Griffin, C. Seigneur, and J.H. Seinfeld, *Secondary organic aerosol - 2. Thermodynamic model for gas/particle partitioning of molecular constituents.* Journal of Geophysical Research-Atmospheres, 2002. **107**(D17).
21. Kusik, C.L. and H.P. Meissner, *Electrolyte activity coefficients in inorganic processing.* Fundamental Aspects of Hydrometallurgical Processes AIChE Symposium Series, 1978. **74**: p. 14-20.
22. Fredenslund, A., J. Gmehling, and P. Rasmussen, *Vapor-liquid equilibrium using UNIFAC*. 1977, New York: Elsevier.
23. Clegg, S.L., J.H. Seinfeld, and E.O. Edney, *Thermodynamic modelling of aqueous aerosols containing electrolytes and dissolved organic compounds. II. An extended Zdanovskii-Stokes-Robinson approach.* Journal of Aerosol Science, 2003. **34**(6): p. 667-690.
24. Clegg, S.L., J.H. Seinfeld, and P. Brimblecombe, *Thermodynamic modelling of aqueous aerosols containing electrolytes and dissolved organic compounds.* Journal of Aerosol Science, 2001. **32**(6): p. 713-738.
25. Czoschke, N.M., M. Jang, and R.M. Kamens, *Effect of acidic seed on biogenic secondary organic aerosol growth.* Atmospheric Environment, 2003. **37**(30): p. 4287-4299.
26. Jang, M.S., B. Carroll, B. Chandramouli, and R.M. Kamens, *Particle growth by acid-catalyzed heterogeneous reactions of organic carbonyls on preexisting aerosols.* Environmental Science & Technology, 2003. **37**(17): p. 3828-3837.
27. Kalberer, M., D. Paulsen, M. Sax, M. Steinbacher, J. Dommen, A.S.H. Prevot, R. Fisseha, E. Weingartner, V. Frankevich, R. Zenobi, and U. Baltensperger,

Identification of polymers as major components of atmospheric organic aerosols. Science, 2004. **303**(5664): p. 1659-1662.

28. Kleeman, M.J., G.R. Cass, and A. Eldering, *Modeling the airborne particle complex as a source-oriented external mixture.* Journal Of Geophysical Research-Atmospheres, 1997. **102**(SEP 20): p. 21355-21372.
29. Kleeman, M.J., *Changes in PM2.5 Due to Changes in Temperature*. 2004, Final Report for the U.S. Environmental Protection Agency Contract # R-82824201-01.
30. Goodin, W.R., G.J. McRae, and J.H. Seinfeld, *A comparison of Interpolation Methods for Sparse Data: Application to Wind and Concentration Fields.* Journal of Applied Meteorology, 1979. **18**: p. 761-771.
31. Cooper, J.A., D.C. Redline, L.N. Sherman, L.M. Valdovinos, L.C. Scavone, and C. Badgett-West, *Final appendix V-G, PM10 source composition library for the South Coast Air Basin, technical report*. 1989, South Coast Air Quality Management District: Diamond Bar, California.
32. Taback, H.J., A.R. Brienza, J. Macko, and N. Brunetz, *Fine particle emissions from stationary and miscellaneous sources in the South Coast Air Basin, technical report*. 1979, California Air Resources Board; KVB Incorporated; Research-Cottrell: Tustin, California.
33. Schauer, J.J., M.J. Kleeman, G.R. Cass, and B.R.T. Simoneit, *Measurement of emissions from air pollution sources. 5. C-1-C-32 organic compounds from gasoline-powered motor vehicles.* Environmental Science & Technology, 2002. **36**(MAR 15): p. 1169-1180.
34. Schauer, J.J., M.J. Kleeman, G.R. Cass, and B.R.T. Simoneit, *Measurement of emissions from air pollution sources. 4. C-1-C-27 organic compounds from cooking with seed oils.* Environmental Science & Technology, 2002. **36**(FEB 15): p. 567-575.
35. Schauer, J.J., M.J. Kleeman, G.R. Cass, and B.R.T. Simoneit, *Measurement of emissions from air pollution sources. 3. C-1-C-29 organic compounds from fireplace combustion of wood.* Environmental Science & Technology, 2001. **35**(MAY 1): p. 1716-1728.
36. Schauer, J.J., M.J. Kleeman, G.R. Cass, and B.R.T. Simoneit, *Measurement of emissions from air pollution sources. 2. C-1 through C-30 organic compounds from medium duty diesel trucks.* Environmental Science & Technology, 1999. **33**(MAY 15): p. 1578-1587.
37. Schauer, J.J., M.J. Kleeman, G.R. Cass, and B.R.T. Simoneit, *Measurement of emissions from air pollution sources. 1. C-1 through C-29 organic compounds from meat charbroiling.* Environmental Science & Technology, 1999. **33**(MAY 15): p. 1566-1577.
38. Hildemann, L.M., G.R. Markowski, M.C. Jones, and G.R. Cass, *Submicrometer Aerosol Mass Distributions of Emissions from Boilers, Fireplaces, Automobiles, Diesel Trucks, and Meat- Cooking Operations.* Aerosol Science and Technology, 1991. **14**(1): p. 138-152.
39. Kleeman, M.J., J.J. Schauer, and G.R. Cass, *Size and composition distribution of fine particulate matter emitted from wood burning, meat charbroiling, and cigarettes.* Environmental Science & Technology, 1999. **33**(20): p. 3516-3523.
40. Kleeman, M.J., J.J. Schauer, and G.R. Cass, *Size and composition distribution of*

fine particulate matter emitted from motor vehicles. Environmental Science & Technology, 2000. **34**(7): p. 1132-1142.

41. Harley, R.A., M.P. Hannigan, and G.R. Cass, *Respeciation of Organic Gas Emissions and the Detection of Excess Unburned Gasoline in the Atmosphere.* Environmental Science & Technology, 1992. **26**(12): p. 2395-2408.
42. Holtzworth, G.C., *Mixing depths, wind speeds, and air pollution potential for selected locations in the United States.* Journal of Applied Meteorology, 1967. **6**: p. 1029-1044.
43. Gharib, S. and G.R. Cass, *Ammonia emissions in the South Coast Air Basin.* 1984, California Institute of Technology, Environmental Quality Laboratory Open File Report 84-2: Pasadena, CA.
44. Matthijsen, J., H. Slaper, H. Reinen, and G.J.M. Velders, *Reduction of solar UV by clouds: A comparison between satellite-derived cloud effects and ground-based radiation measurements.* Journal of Geophysical Research-Atmospheres, 2000. **105**(D4): p. 5069-5080.
45. Harley, R.A., A.G. Russell, G.J. McRae, G.R. Cass, and J.H. Seinfeld, *Photochemical Modeling of the Southern California Air-Quality Study.* Environmental Science & Technology, 1993. **27**(2): p. 378-388.
46. Hildemann, L.M., G.R. Markowski, and G.R. Cass, *Chemical-Composition of Emissions from Urban Sources of Fine Organic Aerosol.* Environmental Science & Technology, 1991. **25**(4): p. 744-759.
47. Houck, J.E., J.C. Chow, J.G. Watson, C.A. Simons, L.C. Pritchett, J.M. Goulet, and C.A. Frazier, *Determination of particle size distribution and chemical composition of particulate matter from selected sources in California, technical report*. 1989, California Air Resources Board; OMNI Environ. Service Incorporate; Desert Research Institute: Beaverton, Oregon.